CO$_2$ ADSORPTION ANALYSIS OF CATION EXCHANGED MORDENITE-TYPE ZEOLITE WITH ALKALI AND ALKALINE EARTH METAL

YEOH ZHI YI

A project report submitted in partial fulfilment of the requirements for the award of Bachelor of Engineering (Honours) Chemical Engineering

Lee Kong Chian Faculty of Engineering and Science
Universiti Tunku Abdul Rahman

April 2020

DECLARATION

I hereby declare that this project report is based on my original work except for citations and quotations which have been duly acknowledged. I also declare that it has not been previously and concurrently submitted for any other degree or award at UTAR or other institutions.

Signature : *YeohZhiYi*

Name : YEOH ZHI YI

ID No. : 15UEB02989

Date : 15th MAY 2020

APPROVAL FOR SUBMISSION

I certify that this project report entitled **"CO₂ ADSORPTION ANALYSIS OF CATION EXCHANGED MORDENITE-TYPE ZEOLITE WITH ALKALI AND ALKALINE EARTH METAL"** was prepared by **YEOH ZHI YI** has met the required standard for submission in partial fulfilment of the requirements for the award of Bachelor of Engineering (Honours) Chemical Engineering at Universiti Tunku Abdul Rahman.

Approved by,

Signature   :

Supervisor   :   DR. LEE ZHI HUA

Date   :   15th MAY 2020

ACKNOWLEDGEMENTS

I would like to thank everyone who had contributed to the successful completion of this project. I would like to express my gratitude to my research supervisor and, Dr. Lee Zhi Hua for his invaluable advice, guidance and her enormous patience throughout the development of the research.

In addition, I would also like to express my gratitude to my loving parents and friends who had helped and given me encouragement during my hard times. I would like to specially thanks Miss Vitiyaa a/p Selva Kumar for helping and supporting me throughout my project. Without their guidance and knowledge, this research would have not come to completion.

ABSTRACT

In this project, the mordenite-type (MOR) zeolite with Si/Al ratio around 5 was used for the CO_2 adsorption analysis. The impact of different temperatures and cation exchange with alkali and alkaline earth metals on CO_2 adsorption of MOR zeolite adsorbent were analysed using Thermogravimetric Analyser (TGA). Raw mordenite (R-MOR) zeolite exhibited the highest maximum CO_2 adsorption capacity of 0.1198 mmol/g, highest maximum CO_2 adsorption rate of 0.0020 mmol/(g·min), maximum N_2 adsorption capacity of 1.0201 mmol/g and highest maximum CO_2/N_2 selectivity of 0.1175 at 30 °C. The CO_2 adsorption properties of R-MOR zeolite were decreased with a rise of temperature. The kinetic study of CO_2 adsorption at different temperatures revealed that R-MOR followed pseudo-first order model at 30 °C; intra-particle diffusion model at 50 °C and 100 °C. Since, R-MOR zeolite exhibited the best performance at 30 °C, following R-MOR zeolite was cation exchanged with alkali and alkaline earth metals and tested at 30 °C. The maximum CO_2 adsorption capacity and maximum CO_2 adsorption rate of the adsorbents followed an order of Ca-MOR> Mg-MOR> Na-MOR> K-MOR> R-MOR. Ca-MOR zeolite showed the highest maximum CO_2 adsorption capacity of 0.4478 mmol/g, highest maximum CO_2 adsorption rate of 0.0075 mmol/(g·min), least maximum N_2 adsorption capacity of 0.2168 mmol/g and highest maximum CO_2/N_2 selectivity of 2.0655 at 30 °C. The X-ray diffraction (XRD) test confirmed the characteristic peaks of the adsorbents before and after cation exchanged were consistent with reference peaks of mordenite zeolite provided in International Zeolite Association. Fourier-transform infrared spectroscopy (FTIR) test exhibited the essential peaks for zeolite material and CO_2 adsorbed peaks in the adsorbents. The structure of the adsorbents showed in Scanning Electron Microscope (SEM) test were nanofiber-like crystal and some amorphous globules made of entangled zeolite fibres. The Energy Dispersive X-ray Analyzer (EDX) result revealed that the adsorbents had a better affinity towards K^+ during cation exchange.

TABLE OF CONTENTS

CHAPTER

LIST OF TABLES

LIST OF FIGURES

LIST OF SYMBOLS / ABBREVIATIONS

M	metals or hydogen cation
n	valence of the metal cation
y	number of water molecules in the structure of zeolite
$\overline{U}_{total}$	total interaction potential energy
M_t	mass of adsorbent at time t, mg
M_0	initial mass of adsorbent before CO_2 adsorption, mg
MW_{CO_2}	molecular weight of CO_2, g/mol
t	time, min
q_e	CO_2 adsorption capacity at equilibrium, mmol/g
q_t	CO_2 adsorption capacity at time of t, mmol/g
k	rate constant of pseudo-first order, min^{-1}
k_s	rate constant of pseudo-second order, mmol/g
k_{id}	diffusion constant of intra-particle diffusion, mmol/(g·$min^{-0.5}$)
C	thickness of boundary layer
d_x	crystallite size, nm
λ	wavelength of X−ray, (CuKα =0.15406nm)
θ	Bragg angle, rad/ °
T	Si or Al
p_{CO_2}	Partial pressure of CO_2
p_{N_2}	Partial pressure of N_2
AlO_4	aluminate
Ca-MOR	calcium exchanged zeolite
CCS	carbon dioxide capture and storage
$CaCl_2$	calcium chloride anhydrous
CO_2	carbon dioxide
$FWHM$	full width at half maximum, rad
FTIR	Fourier-transform infrared spectroscopy
GHGs	greenhouse gases
H_2O	distilled water
KCl	potassium chloride

K-MOR	potassium exchanged zeolite
Mg-MOR	magnesium exchanged zeolite
$Mg(NO_3)_2$	magnesium nitrate hexahydrate
MOR	mordenite
$Mg(OH)_2$	magnesium hydroxide
NaCl	sodium chloride
Na-MOR	sodium exchanged zeolite
R-MOR	raw zeolite
SEM-EDX	scanning electron microscope - energy dispersive x-ray analyzer
Si/ Al	ratio of silica to aluminium
SiO_4	silicate
TEOS	tetraethyl orthosilicate
TGA	thermogravimetric analyser
XRD	X-ray diffractometer

LIST OF APPENDICES

CHAPTER 1

INTRODUCTION

1.1   General Introduction

Over the year, the global temperature has increased rapidly and this phenomenon is known as global warming. Global warming is mainly caused by the emissions of greenhouse gases (GHGs) consist of carbon dioxide (CO_2), water vapour, methane and nitrous oxide. However, the major contributor to global warming is the emissions of CO_2 from industrial sector. This statement can be proven by the graph shown in Figure 1.1 where the global temperature anomaly occurred after the industrialization from 18th to 19th century. The overall climate change is + 0.18 °C/ decade since 1980 and + 1 °C for several recent years. This temperature anomaly is estimated to be going uphill to an increment of 2 °C by 2065 year (Berkeley Earth, 2019). To prevent this undesirable situation, Paris Agreement is adopted within the United Nations Framework Convention on Climate Change (UNFCCC) on 12 December 2015 to fight climate change. The goal of Paris agreement is to limit rise in temperature to 1.5 °C. Parties that ratified the treaty are required to implement a set of mandatory measures to limit the CO_2 emissions annually and revisit their pledges every five years.
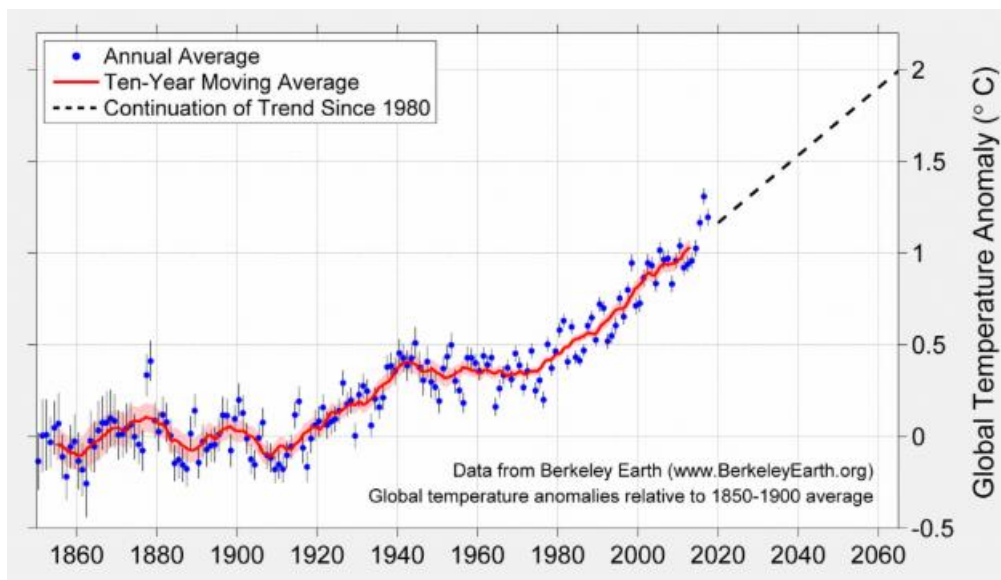
Figure 1.1: Global Temperature Anomaly for 1850-2017 (Berkeley Earth, 2019).

Regards to the environmental issue mentioned above, an emerging technology such as CO_2 capture and storage (CCS) is developed to reduce CO_2 emissions from energy sector. The basic concept of CCS is to capture CO_2 emissions before it is released into atmosphere, transport and inject the compressed CO_2 into the selected geological rock formation underground or depleted oil and gas fields (Nediljka and Karolina, 2019). The CCS technology can be classified into three types such as post-combustion, pre-combustion and oxy-fuel combustion technologies. Post-combustion is the most common and applicable technology in capturing the CO_2 emission from power plant. The post-combustion sorbents can be further classified into dry, wet, membrane-based and cryogenics techniques. Table 1.1 listed down the advantages and drawbacks of the techniques in post-combustion process (Lee and Park, 2015).

Table 1.1: Advantages and Limitation of the Techniques Used in Post Combustion Process (Lee and Park, 2015).

Technique	Advantages	Limitations
Dry adsorption	- Simple device - Positive environmental impact - Energy-efficient	Poor treatment for large emission volume
Wet adsorption	- Effective treatment for large emission volume - Able to change CO_2 density	- Require high energy for absorbent regeneration - Absorbent must be heated - Corrosion problem - Slow solid-gas reaction
Membrane-based	- Simple device - User friendly - Low energy consumption	- High cost module - Not durable
Cryogenics	- Low investment cost - High reliability	- High energy consumption - Aging of membrane

In this study, priority is given to the dry adsorbents because the temperature range for the use of solid adsorbents are wider than liquid absorbent. The temperature for solid adsorption process can be ranged from ambient temperature till 700 °C. Under low temperature adsorption (< 200 °C) categories, the solid adsorbents consist of zeolite, carbon-based, metal organic framework, alkali metal carbonate and amine-based solid adsorbents (Wang, et al., 2011). Among these solid adsorbents, zeolite is chosen for a further study because of its low cost and high thermal stability.

Zeolite can be found in nature and synthesized artificially. The crystalline aluminosilicates structure of zeolite consists of SiO_4 and AlO_4 tetrahedra that shared O-corner atoms in different ways to build a crystalline lattice with well-defined pores and channels. The extra negative charge introduced by aluminium atoms onto the zeolite framework can be balanced off through the exchangeable cations such as alkali, alkaline earth or transition metals.

1.2   Importance of the Study

In order to remove the CO_2 from industrial effluent gases, solid adsorbent is developed to capture CO_2 emission. Zeolite-based adsorbent is proven to be a promising solid adsorbent because it offers several advantages such as the molecular sieving effect and strong interactions between CO_2 with cations in the zeolite framework. Many studies related to modification of zeolite based adsorbent through cation exchange to enhance the CO_2 adsorption capacity had been done by other authors. Their studies are more on the evaluation of CO_2 adsorption capacity for low Si/Al ratio zeolite (NaA, NaX and NaY) and high Si/Al ratio zeolite (ZSM-5). The lower ratio of Si/Al in zeolite has a higher basicity which induces stronger interaction between CO_2 and zeolite that can result in high value of CO_2 adsorption. However, the high amount of aluminium tetrahedral also provides an unstable site that would be attacked by acid and water vapour (steam) and reduce the overall stability of zeolite, vice versa for high Si/Al ratio zeolite. Thus, an intermediate Si/Al ratio of MOR zeolite is introduced.

1.3   Problem Statement

The Bensafi, Chouat and Djafri (2017) suggested that the synthesized alkali exchanged mordenite with presence of N,N-dimethylaniline has an increment of CO_2 adsorption capacity at 25 °C in sequence of Cs-MOR > K-MOR > Na-MOR. The investigation of interaction between CO_2 with Na, K, and Ca-exchanged mordenite using FTIR had been performed in Villarreal, Castillo-Villalon, and Ramirez (2017). To my best knowledge, no study has been carried out for the impact of temperature on the CO_2 adsorption capacity and CO_2 adsorption rate of MOR zeolite as well as the CO_2 adsorption over cation exchange MOR zeolite with alkaline earth metals. Herein, the kinetic study of CO_2 adsorption at different temperatures and influence of alkali and alkaline earth metal ions on the CO_2 adsorption capacity and CO_2 adsorption rate for MOR zeolite are presented.

1.4   Aim and Objectives

The aim of this project is to investigate the CO_2 adsorption capacity and CO_2 adsorption rate of MOR zeolite at various temperatures and after the cation exchange with alkali and alkaline earth metals. The objectives of this project are:

(i)   To study the CO_2 adsorption capacity and CO_2 adsorption rate of MOR zeolite at different temperatures using TGA.

(ii) To study the CO_2 adsorption capacity and CO_2 adsorption rate of cation exchanged MOR zeolite using TGA.

(iii) To characterize MOR zeolite and cation-exchanged MOR zeolite with the aid of XRD, FTIR and SEM-EDX.

1.5   Scope and Limitation of the Study

The scopes of this study is to evaluate the impact of temperature on CO_2 adsorption capacity of MOR zeolite. Then, MOR zeolite is cation exchanged with Na^+, K^+, Ca^{2+} and Mg^{2+} to further improve the CO_2 adsorption capacity. The structural and composition changes of cation exchanged MOR zeolites are determined using XRD, FTIR and SEM-EDX.

The limitations of this study include desorption and regeneration with and without the presence of water are not include in the CO_2 analysis. Besides,

pure CO_2 is used for the analysis of CO_2 adsorption capacity. Indeed, the amount of CO_2 in flue gas mixture is 10-15 % and the rest are composed of nitrogen, water and oxygen (Dunstan, et al., 2016).

1.6   Contribution of the Study

Upon completion of this study, the optimum temperature for MOR zeolite to achieve highest CO_2 adsorption capacity is determined. The transport mechanism of CO_2 into MOR zeolite at different temperatures are identified. By having this understanding, the CO_2 adsorption analysis for the cation exchanged MOR zeolites were evaluated under the optimum temperature to find the most feasible MOR zeolite to capture CO_2.

1.7   Outline of the Report

Chapter 1 introduced the cause of global warming and the existing CO_2 capture technologies. Under the same chapter, importance of study, problem statement, aims and objectives, contribution of the study as well as scope and limitation of the study are elaborated. Chapter 2 is the literature review of some facts and related works done by other authors. Chapter 3 demonstrates the methodology and work plan for this study. It involves the type of materials and equipment used, research flow diagram, adsorbent preparation and type of kinetic models that will be used in subsequent chapter. Chapter 4 presents the results obtained from TGA, XRD, FTIR and SEM-EDX and their discussion as well as the kinetic study of CO_2 adsorption at different temperatures. Chapter 5 is conclusion and recommendations for this study and future research.

CHAPTER 2

LITERATURE REVIEW

2.1   Introduction

This chapter discussed some relevant literature reviews on type of solid adsorbents, properties of natural and synthetic zeolites, factor influencing the CO_2 adsorption capacity on zeolite and mechanism of CO_2 adsorption on zeolite.

2.2   Type of Adsorbents

To solve the greenhouse problem, various types of solid adsorbents have been synthesized and modified to capture the CO_2 from its emission points. Table 2.1 summarized the advantages and limitations of the general solid adsorbents.

Table 2.1: Advantages and Limitations of the General Solid Adsorbents (Lee and Park, 2015).

Type of Adsorbents	Advantages	Limitations
Zeolite and silica materials	• Low production cost • High CO_2 adsorption capacity and selectivity at low ratio of Si/Al	• Sensitive to water vapour/ steam (moisture adsorption problem) that would inhibit CO_2 adsorption capacities • High energy consumption for CO_2 desorption
Calcium oxide	• Low production cost • Low regeneration energy • Able to adsorb CO_2 at high temperature	• Sintering of adsorbent at high exothermic process cause the loss of reversibility for carbonation reaction • CO_2 adsorption capacity reduce after each cycle
Metal organic frameworks (MOF)	• Large specific surface area range from 1000-10000 m^2/g • High CO_2 adsorption capacity at high pressure	• High production cost • Poor CO_2 adsorption capacity at low partial pressure • Moisture adsorption problem

Table 2.1 (Continued)

Type of Adsorbents	Advantages	Limitations
Activated carbon	• High thermal stability • Low cost • Hydrophobic structure with low sensitive to water • Durable under acid and alkali condition	• Low CO_2 adsorption capacity at low partial pressure
Alkali metal carbonate based	• Low cost	• Poor regeneration and cyclic performance

The commercially used or analysed solid adsorbents can be classified into low (< 200 °C), intermediate (200 - 400 °C), and high temperature solid adsorbents (> 400 °C). Table 2.2 compared the CO_2 adsorption capacities of the general adsorbents under adsorption pressure of 1 atm.

Table 2.2: General Adsorbents' CO_2 Adsorption Capacities under Adsorption Pressure of 1 atm (Wang, et al., 2011).

Categories of Temperature	Adsorbent Type	Adsorption Temperature (°C)	CO_2 adsorption capacities (mmol/g)
Low	Zeolite	≤ 100	≤ 4.9
	MOF	≤ 100	≤ 4.5
	Carbon-based	≤ 80	≤ 3.5
	Alkali metal carbonate based	≤ 120	≤ 9.4
Intermediate	Layered double hydroxide based	200-400	≤ 1.4
High	Alkali ceramic based	500-600	≤ 6.5
	Calcium oxide	600-700	≤ 11.6

By relating the relation between properties and CO_2 adsorption capacities of the general solid adsorbents, it can be concluded that the most promising solid adsorbents are CaO and alkali metal carbonate based adsorbents at high and low

temperature operation respectively. The alkali based carbonate has a poor regeneration and cyclic performance to capture CO_2, while high adsorption temperature of CaO may accidentally cause sintering of adsorbent at high exothermic process which would lead to loss of reversibility for carbonation reaction as CO_2 adsorbent. Thus, zeolite with the second large CO_2 adsorption capacity become a potential CO_2 solid sorbent to be further investigated in this project. In real industry case, the challenges such as water sensitive issue and high energy consumption for desorption in zeolite should be further studied. Díaz, et al. (2008) reported that the Cs- treated Y zeolite exhibited an increasing CO_2 retention capacity after water adsorption-desorption testing at 100-200 °C. This study provides an alternative way to improve properties of zeolite as a potential CO_2 adsorbent.

2.3   Properties of Natural and Synthetic Zeolites

In 1756, a Swedish mineralogist named Axel Fredrik Cronstedt discovered a natural zeolite through the observation of the boiling zeolite stone in rapid heat treatment. The term "zeolite" was formed from Greek words: "zeo" = boil; "lithos" = stone (Mohau, et al., 2017). According to 911Metallurgist (2017), about 40 type of natural zeolites were identified in 1980's and over 150 type of artificial zeolites have been synthesized and verified under International Zeolite Association. Generally, zeolite is a microporous and hydrated crystalline aluminosilicates that consists of SiO_4 and AlO_4 tetrahedra. Both of the tetrahedra will join at corner through the sharing oxygen atoms and form a 3-D framework of zeolite with channels, cages and cavities as illustrated in Figure 2.1. After the joining of both tetrahedral, there will be an overall negative charge on the aluminosilicate framework because the cation charge for aluminium and silicon ion are 3+ and 4+ respectively. To balance off this negative charge, cation exchange with other metal ion will be performed. This availability of cation exchange makes zeolite as a useful catalyst in many industrial applications, especially in petrochemical industry. Besides, zeolite can be classified under the class of "molecular sieves" due to the presence of large voids in between interconnected channel and cages in zeolite framework. The large voids in framework allow resident ions and molecules to drift in and out

of the structure easily and the specific density of zeolite is low under this condition.
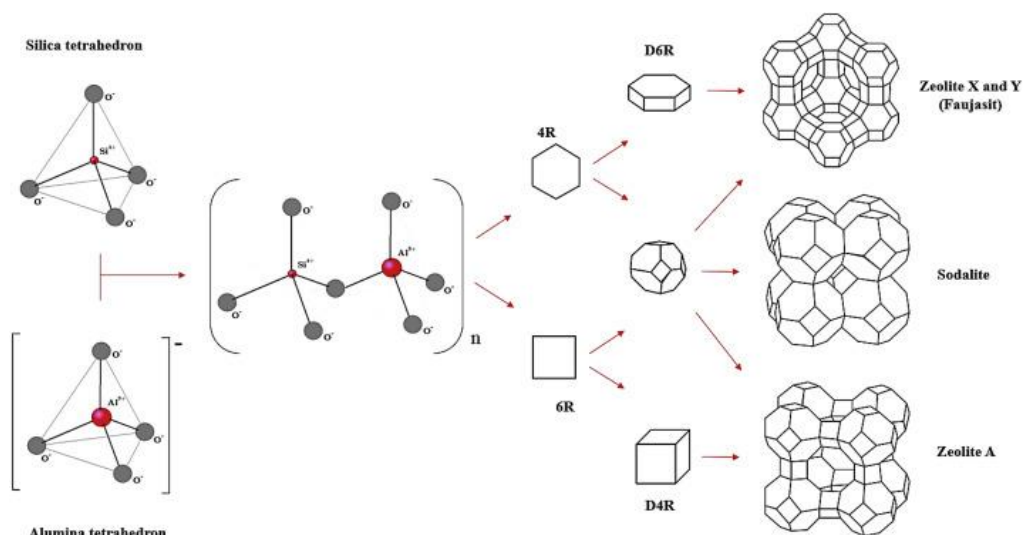
Figure 2.1: Building Unit of Zeolite Structure (Salehi and Anbia, 2017).

The general chemical formula for zeolite is shown in Eq. 2.1.

$$M_2/nO \cdot Al_2O_3 \cdot xSiO_2 \cdot yH_2O \qquad (2.1)$$

where

M= metals or hydogen cation

n = valence of the metal cation

y = number of water molecules in the structure of zeolite

The natural type of zeolites are obtained from the reaction of volcanic glass and saline water at temperature range of 27 °C - 55 °C within pH of 9 -10. It takes long time to complete this natural reaction, yet the uniformity and purity of natural zeolites are not high due to contamination by other minerals in geological environments. The contamination inside zeolite would increase complexity of pre-treatment process in order to obtain a useful zeolite. Therefore, synthetic zeolite is introduced.

To synthesize a zeolite, the source of aluminium can be obtained from chemical precursor; while the silica source can be extracted from chemical precursor or natural sources. Example of chemical precursors for aluminium

sources are aluminium nitrate, aluminium chloride and sodium aluminate. The commercially used aluminium precursor is sodium aluminate due to its versatility applications. For instance, addition of sodium aluminate as coagulant agent in water softening system for suspended solid removal, accelerator to solidify concreate, auxiliary refining and retaining agent in paper industry and intermediate for production of zeolite (AZoM, 2006). From the work done by Hisham, et al. (2011), the surface area of synthesized nano-size ZSM-5 zeolite from three different aluminium precursors was increased in order of aluminium nitrate< aluminium chloride < sodium aluminate. Clearly, the higher surface area of synthesized zeolite from sodium aluminate is important for the CO_2 adsorption.

On the other hand, different type of silica chemical precursors would affect the properties of synthesized products. Among the silica chemical precursors such as sodium silicate solution, colloidal silica, tetraethyl orthosilicate (TEOS), fumed silica and others, sodium silicate solution is commercially used in industry and laboratory. However, Aimen Isa (2018) suggested that colloidal silica performed better than sodium silicate in synthetization an octahedral shape of NaY zeolite. It showed that NaY zeolite was successfully synthesized without an addition of NaY seeds. Furthermore, the higher amount of Na^+ ions in colloidal solution would assist the stabilization of highly open structure NaY zeolite and increase the solution's alkalinity to allow higher solubility of aluminosilicate to form crystalline NaY zeolite. Xu, et al (2010) reported that fumed silica could replace the conventionally used TEOS as a silica source to synthesis a pure silica ITQ-13 zeolite. This is because the fumed silica exhibited several advantages such as low cost with equivalent purity as TEOS, exemption from hydrolysis process for the gel making, and low ratio of H_2O/ Si and high crystallization temperature for crystallization process. The fumed silica synthesized ITQ-13 zeolites had excellent thermal stability at 428 and 448 K, while organic SDA and fluorine that occluded in zeolite can be removed when calcined above 803 K.

Although the sodium silicate solution is widely used for preparation of gel, catalyst and zeolite, the cost for chemical precursor is still consider as high compared to the natural silica sources in large scale production of synthetic zeolite. The possible natural silica sources are those waste materials such as

kaolin, rice husk ash, fly ash, municipal solid waste incineration ashes and other sources.

Kaolin is a white clay that rich in kaolinite with a structure of combined single SiO_4 tetrahedral sheet and single AlO_6 octahedral sheet (Petrov and Michalev, 2012). It is cheap and environment friendly, but composed of many impurities. Thus, pre-treatment is required to convert kaolin into a more reactive metakaolin, which may contribute to the cost preparation. Rice husk is a waste from agricultural industry with little or no commercial value. However, the high grade of amorphous silica in rice husk is an excellent source of silica. High amount silica oxide can be extracted out from rice husk after treat the rice husk with a thermal and acid treatment to become rice husk ash. Fly ash is an inorganic residue from coal combustion in power plant. It contains ash viz., SiO_2 and Al_2O_3, which are the required constituents for aluminosilicate zeolite. Another reason to utilize fly ash as raw material for zeolite synthesis is the similarity in chemical composition between fly ash and some volcanic rocks. As mentioned before, natural zeolite is a volcanic mineral. This finding therefore leads to major attempts to synthesize zeolite using the fly ash's silica source from 1990 onwards. Through a wise utilization of these waste materials in the synthesis of zeolite, the environmental problems can be mitigated. Whereby, waste to wealth concept is applied.

Other than the selection of raw materials, the physicochemical, catalyst and gas adsorptive characteristics of synthesized zeolite can be influenced by the ratio of silica to alumina. The Si/Al ratio in zeolite are divided into three classes: low, intermediate and high silica zeolite. The most commercial adsorbents of low silica zeolite are Linde-type A and NaX zeolite. Both zeolites have highly saturated aluminium contents with Si/Al ratio of 1 - 1.5. In the aluminosilicate framework, high aluminium contents will increase the cation exchange capacity and the adsorption capability of the zeolite. At the same time, the high amount of aluminium tetrahedral also provides an unstable site that would be attacked by acid and water vapour (steam) and reduce the overall stability of zeolite. To improve the stability of zeolite, more silicon contents are required by introducing an intermediate silica zeolite with Si/ Al = 3 - 5. The commercially used zeolites under this class are clinoptilolite and modernite zeolite which exhibit a good thermal and acid stability. The surface properties

of low and intermediate silica zeolites are heterogeneous and hydrophilic. For high silica zeolite, the Si/Al ratio is greater than 10. The surface of high silica zeolite is homogeneous with a high organophilic-hydrophobic selectivity. The commercially used high silica zeolites are ZSM-5 and beta zeolite. To have a brief understanding on some commonly used zeolites, the type of zeolite and their Si/Al ratio are depicted in Figure 2.2 and 2.3.
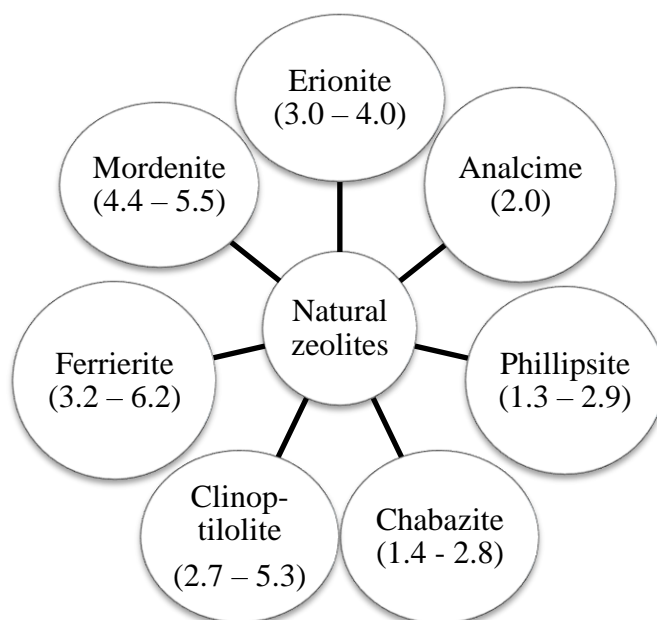
Figure 2.2: Type of natural zeolites with their Si/Al ratio.
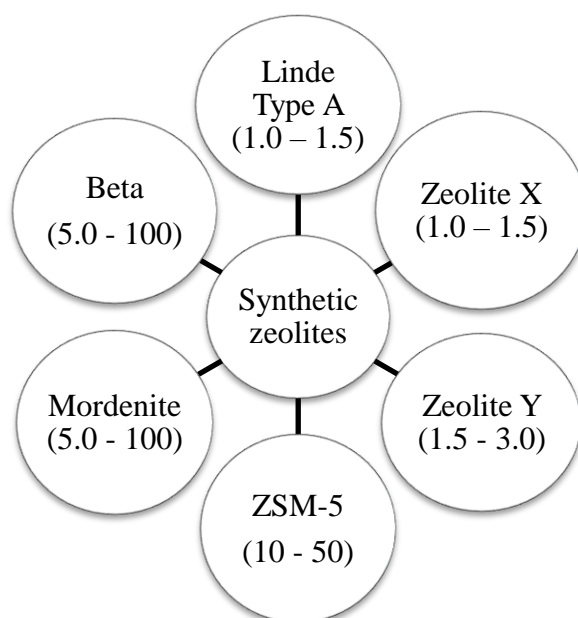
Figure 2.3: Type of synthetic zeolites with their Si/Al ratio.

2.4　　Influence Factors In the CO_2 Adsorption Capacity on Zeolite

There are several factors that would influence the CO_2 adsorption capacity of zeolite. First factor is the Si/Al ratio of zeolite. As the Si/Al ratio decreases, the CO_2 adsorption capacity increases. This can be attributed to the presence of more Al-atoms in framework that increase the number of charged sites and the surface basicity of zeolite at low Si/Al ratio. This is important to CO_2 that has the highest polarizability and quadrupole moment among the gases listed in Table 2.3. It is worthwhile to mention that definition of polarizability is how easily the distortion of an electron cloud by an electric field (Chemical Dictionary, 2017). While, quadrupole moment is defined as the tendency of quadrupole to rotate about an axis (Chemistry LibreTexts, 2019). When the number of charged sites increases, the electric field on the zeolite pores increases as well that can induce a stronger attraction between CO_2 and zeolite. This fact is supported by the result in Megías-Sayago, et al. (2019), H-ZSM-5-D zeolite (Si/Al ratio = 43) had the greatest CO_2 adsorption capacity of 1.033 mmol/g as compared to H-ZSM-5-C zeolite (Si/Al ratio = 55), H-ZSM-5-B zeolite (Si/Al ratio = 155) and H-ZSM-5-A zeolite (Si/Al ratio = 226) which had CO_2 adsorption capacity of 0.968 mmol/g, 0.790 mmol/g and 0.745 mmol/g respectively at 40°C.

Table 2.3: Properties of Some Adsorbate Gases (Aslı ERTAN, 2004).

Adsorbate Gas	Molecular Weight (g/ mol)	Kinetic Diameter (Å)	Polarizability ($\times 10^{-25}$ cc)	Quadrupole Moment ($\times 10^{-26}$ esu-cm^2)
CO_2	44.01	3.30	26.5	4.30
CO	28.01	3.76	19.5	2.50
O2	32.00	3.46	17.6	0.39
N_2	28.01	3.64	15.8	1.52
CH_4	16.04	3.80	26.0	0

Second factor is the basicity and strength of electric field in zeolite. The basic strength of zeolite can be enhanced through an exchangeable of electropositivity cation to allow strong capitation of acidic CO_2. In general, the negative charge (-1) on zeolite framework introduced by aluminium tetrahedral

can be balanced off when extra cations are exchanged within the cavities in zeolite. When more electropositive cation is exchanged into cavities, the electron density of the framework oxygen in zeolite increases and thus increase the basic strength of the zeolite. The electropositivity of elements increase in the order of Mg< Ca< Na< K. To support this fact, the study in Yang, Kim and Ahn (2010) revealed that the CO_2 adsorption capacity of adsorbents increase in the order of Mg-BEA< Cs-BEA≈ Ca-BEA< Ba-BEA< Li-BEA < K-BEA. In contrast, the study in Aguilar-Armenta, et al. (2001) indicated that the basicity of the framework oxygen in clinoptilolite zeolite increased after the substitution of Na^+ and K^+ by Ca^{2+}. This might due to the occlusion of basic metal oxide. It is suggested that basic strength for the basic sites of rare earth oxides and alkaline earth oxides are stronger than those of ion-exchanged.

Third factor is the polarizing power, distribution, size and number of exchangeable cations. The polarizing power of exchangeable cation is inversely proportional to its ionic radius. The penetration of small exchangeable cation within channel of zeolite is more easily that would has stronger interaction with CO_2. This is in agreement with result in Yamazaki, et al. (1993), the total interaction potential energy that contribute to CO_2 adsorption decreases with the increase in ionic radius in M-ZSM-5 (Li, Na, K, Rb, Cs) where the exothermic $\overline{U}_{total}$ for Li-ZSM-5, Na-ZSM-5, K-ZSM-5, Rb-ZSM-5 and Cs-ZSM-5 are 53.55 kJ/mol, 50.60 kJ/mol, 46.90 kJ/mol,45.00 kJ/mol and 42.06 kJ/mol respectively. Sometimes, the acid –base effect is in contrary with the polarizing power of zeolite. The study in Walton, Abney and Douglas LeVan (2006) revealed that the CO_2 adsorption capacity of alkali metal exchanged NaY and NaX zeolite increase in order of of Cs < Rb ≈ K < Li ≈Na and Cs < Rb < K < Na < Li respectively. The largest size cation, Cs showed a strong interaction between CO_2 and zeolite because it is the most electropositive of the stable element in Group 1A and exhibited a strong basic attraction toward the weakly acid $CO_2.$ While, the smallest size cation, Li provided a shorter distance for interaction with the centre of mass of the adsorbate would attract the acidic CO_2 more strongly in the electrostatic interactions within zeolites. In the adsorption capacities of CO_2, the ion-quadrupole interaction is dominant while the acid-base effect was limited by steric factor. The distribution of exchangeable cation in different sites with zeolite framework also influence the CO_2 adsorption

capacity by changing its heterogeneous character. Two common locations for the extra-frame work cation are channel wall sites and intersection sites. According to Grajciar, et al. (2012), the exchangeable cations that located in channel wall sites (top or inside a ring on the surface of channel) would has lower ability to bind adsorbate molecule than cations located at intersection sites (edge of two intersecting channels). This is due to the possibility of cations burry deeper into the channel surface when the interaction between cations with framework oxygen atoms is too strong and reduce the opportunity for the cations to capture the CO_2. Besides, the number exchangeable cations in zeolite framework also plays an important role in the CO_2 adsorption process. The more number or concentration of cations in zeolite can improve its CO_2 adsorption capacity.

Fourth factor is the formation of carbonates on zeolite. During the CO_2 adsorption process, different types of carbonate will form at zeolite surface when chemisorption occurs. The formation of carbonate would hinder the physisorption of CO_2 and thus reduce the CO_2 adsorption capacity of zeolite by limiting the accessibility of CO_2 at a great part of zeolite as illustrated in Figure 2.7 under subsection 2.5.

Fifth factor is the presence of water during CO_2 adsorption process. The attraction of exchangeable cations in zeolite framework is more favour towards the polar water molecule that could reduce the CO_2 adsorption capacity. The strength and heterogeneity of the electric field in framework was reduced with the presence of water as observed in the result obtained from Brandani and Ruthven (2004). Moreover, water molecules support the formation of bicarbonates (a strongly bound CO_2) on zeolite surface that would reduce the CO_2 adsorption capacity and increase the temperature required during CO_2 desorption process.

Last factor is the pressure and temperature during CO_2 adsorption process. The zeolite exhibits greatest CO_2 adsorption capacity at high pressure and low temperature conditions. Bonenfant, et al. (2008) indicated that CO_2 adsorption capacity of zeolite depends on the cationic density at low pressure, whereas the volume of pore on zeolite has dominant effect at high pressure. This fact is support with the result in Walton, Abney and Douglas LeVan (2006) as shown in Figure 2.4. In parallel, the CO_2 adsorption capacity of zeolite decreases

with an increase in temperature. At high temperature, the internal energy of CO_2 increases might induce a higher mobility of CO_2 that decrease trapping or interaction of CO_2 and basic sites of zeolite. The study in Gunawan, Wijiyantia, and Widiastuti (2018) showed that the CO_2 adsorption capacity zeolite-Y-templated carbon (ZTC) at 30 °C, 40 °C, and 50 °C are 2.39 mmol/g, 1.35 mmol/g, and 0.82 mmol/g respectively. Meanwhile, kinetic study at different temperatures indicated that the CO_2 adsorption process at 30 °C and 40 °C followed the pseudo-second order model; at 50 °C followed intra-particle diffusion.
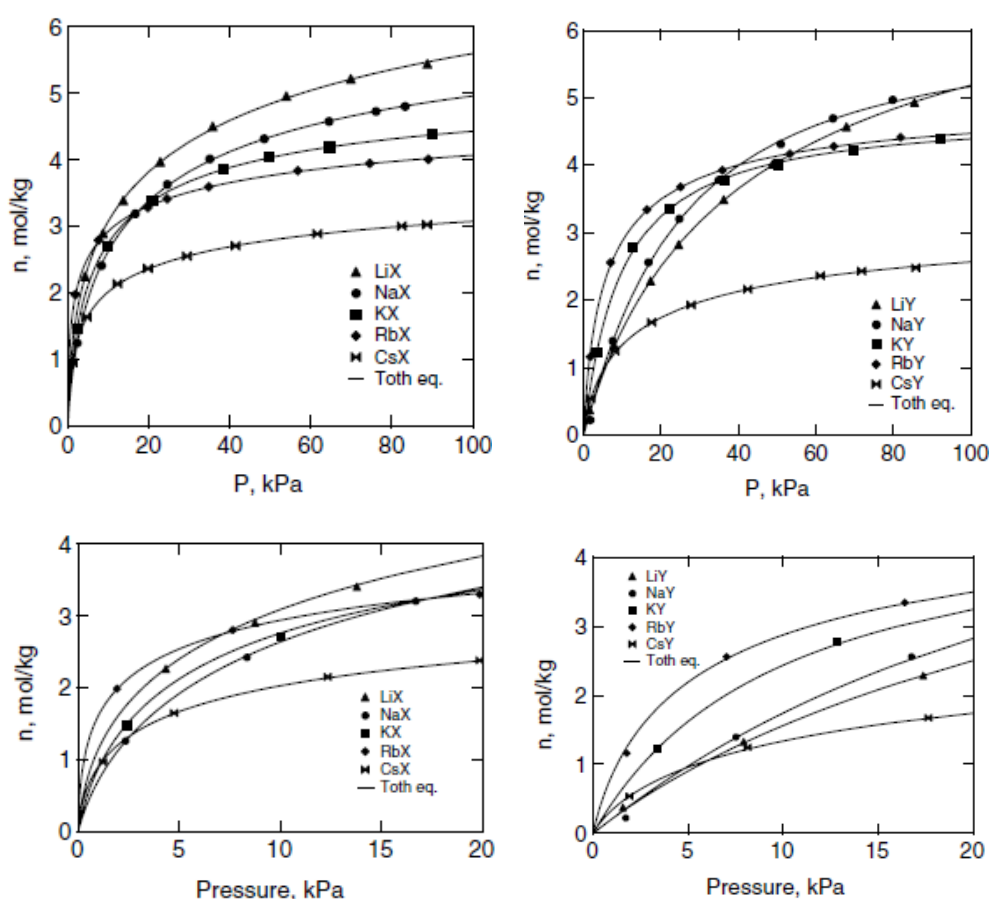
Figure 2.4: Adsorption isotherms for CO_2 at 25 °C on cation exchanged zeolite X and Y at high pressure and low pressure (Walton, Abney and Douglas LeVan, 2006).

The expected of CO_2 adsorption capacity for various type of zeolite-based adsorbent was summarized by Younas, et al. (2016) in Figure 2.5.

Table 4 Physical properties and adsorption capacity of different zeolites

Sorbent	Temperature (°C)	Pressure (atm)	Ads. capacity (mmol g^{-1})	Experimental procedure	References
NaX	32	0.28	5.71	Gravimetric analysis	Bonenfant et al. (2007)
NaX	30	P$_{atm}$	4.20	GC	Li et al. (2013)
NaX (binderless)	25	0.5	4.80	Gravimetric analysis	Yu et al. (2012)
NaX (binderless)	25	0.4	4.50	Gravimetric analysis	Yu et al. (2012)
CaX	30	P$_{atm}$	3.40	GC	Li et al. (2013)
CaX (binderless)	25	1	4.90	Gravimetric analysis	Yu et al. (2012)
CaX (binderless)	25	0.4	3.50	Gravimetric analysis	Yu et al. (2012)
KX (binderless)	25	1	5.00	Gravimetric analysis	Yu et al. (2012)
KX (binderless)	25	0.4	4.50	Gravimetric analysis	Yu et al. (2012)
CaA	30	P$_{atm}$	2.60	GC	Li et al. (2013)
NaA	30	P$_{atm}$	2.40	GC	Li et al. (2013)
NaY	32	1	5.50	Gravimetric analysis	Choudhary et al. (1995)
NaM	25	1	2.95	Gravimetric analysis	Choudhary et al. (1995)
Zeolite 13X	20	0.15	2.63	Fluidized bed	Harlick and Tezel (2004)
	22	1.5	4.90		
Zeolite 13X	22	1	4.61	Fluidized bed	Cavenati et al. (2004)
Zeolite 13X (Binderless)	40	5	4.70	GC	Silva et al. (2014)
Zeolite 13X	25	1	4.66	Fluidized bed	Cavenati et al. (2004)
Miso-LTA	25	1	5.45	TGA	Chen and Ahn (2014)
Micro-LTA			4.77		
Silicalite	30	0.15	0.48	Calorimeter-volum. apparatus	Dunne et al. (1996)
Silica zeolite (CHA)	0	1	4.40	GCMC simulations	Pham et al. (2014)
Na-ZSM-5	30	1	0.75	GC	Katoh et al. (2000)
Molecular sieve 13X	25	1	2.8–3.6[a]	PSA	Siriwardane et al. (2001)
Molecular sieve 13X	20	0.15	2.18	Fluidized bed	Kamiuto et al. (2002)
Molecular sieve 4A	25	1	2.3–3.1[a]	PSA	Siriwardane et al. (2001)
Molecular sieve 4A	20	0.15	1.65	–	Kamiuto et al. (2002)
T-type zeolite	15	1	4.01	GC	Jiang et al. (2013)
Erionite (ZAPS)	17	0.26	3.00	–	Bonenfant et al. (2007)
Mordenite (ZNT)	17	0.26	1.80	–	Bonenfant et al. (2007)
Clinoptilolite (ZN-19)	17	0.26	1.70	–	Bonenfant et al. (2007)
NCW[b]	5	0.4	2.08	Vol. and Isothermal ads.	Ertan (2004)
13X	5	0.9	6.30	Vol. and Isothermal ads.	Ertan (2004)
5A	5	0.7	5.46	Vol. and Isothermal ads.	Ertan (2004)
HY-5	22	1	1.13	Fluidized bed	Harlick and Tezel (2004)
HZSM-5-30	22	1	1.90	Fluidized bed	Harlick and Tezel (2004)
HiSiv 3000	22	1	1.44	Fluidized bed	Harlick and Tezel (2004)
ZSM-5[c]	40	0.1	0.32	GC	Li et al. (2013)
ZSM-5	30	1	1.60	GC	
H-SSZ-13	25	1	3.98	Gravimetric analysis	Hudson et al. (2012)
Cu-SSZ-13	25	1	3.75	Gravimetric analysis	Hudson et al. (2012)

Figure 2.5: CO$_2$ adsorption capacity for various type of zeolite-based adsorbent (Younas, et al., 2016).

In short, factors such as Si/Al ratio, basicity and strength of electric field in zeolite, polarizing power, distribution, size and number of exchangeable cations, formation of carbonates on zeolite, presence of water and pressure and temperature during CO$_2$ adsorption process should be taken into consideration when determine the CO$_2$ adsorption capacity of zeolite.

2.5 Mechanism of CO_2 Adsorption on Zeolite

The mechanism of CO_2 adsorption on zeolite can be physisorbed or chemisorbed or both. A physisorption occurs when CO_2 is attracted to the pore walls within surface of zeolite by Van der Waals forces. The physisorbed CO_2 can be detected using FTIR technique and heat of adsorption method. The rule of thumb for physisorbd CO_2 is the absence of IR peak around 2350 cm^{-1} and heat of adsorption lower than 80 kJ/mol. The heat of adsorption can be determined through two methods such as thermodynamic Clausius–Clapeyron equation and calorimetric method. The information required for Clausius–Clapeyron equation can be obtained through Micrometrics ASAP 2020 apparatus, whereas Tian–Calvet-type microcalorimeter is the commonly equipment to obtain the heat of adsorption in calorimetric method. Figure 2.6 depicted the retaining of CO_2 on zeolite in the phenomena of physisorption and chemisorption.
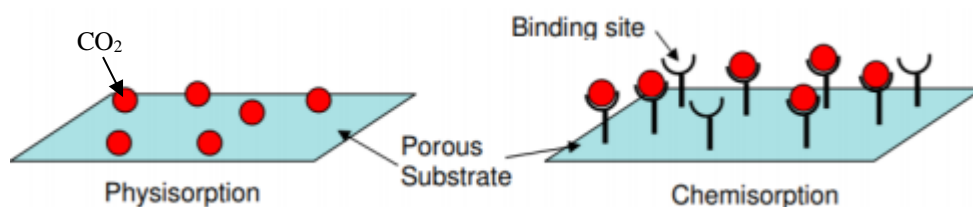
Figure 2.6: Physisorption and Chemisorption for CO_2 molecules (Berger and Bhown, 2011).

A chemisorption occurs when a covalent bond (carbonate) is formed through the sharing of valance electrons between CO_2 and cation on zeolite. To be more detailed, the formation of monodentate carbonate at surface of zeolite as a result of chemisorption is described in Figure 2.7. Initially, CO_2 is polarized when CO_2 interacts with the neighbouring Ca^{2+}. The polarized carbon atom of CO_2 shall attack the oxygen atom that bridged aluminium and silicon atoms. This leads to the breakage of aluminium-oxygen bond and form a monodentate carbonate at zeolite surface (Bonenfant, et al., 2008).
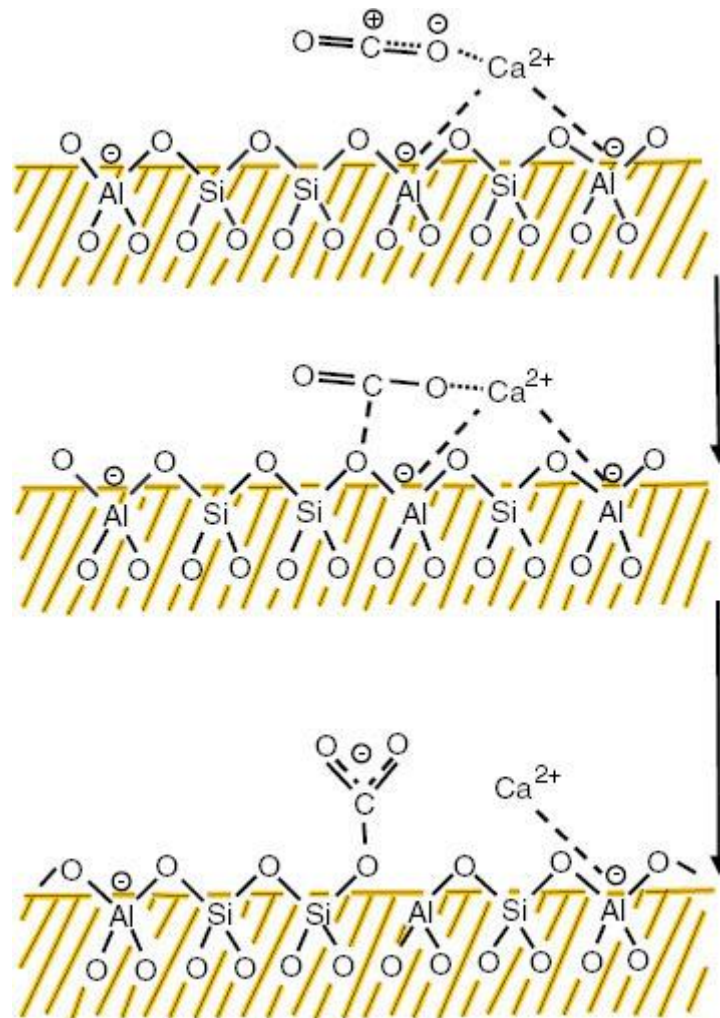
Figure 2.7: Formation of Monodentate Carbonate at surface of zeolite (Bonenfant, et al., 2008).

CHAPTER 3

METHODOLOGY AND WORK PLAN

3.1 Materials and Apparatus

The specific type of materials, apparatus and instruments required for this project were listed in the following subsection.

3.1.1 Materials and Chemicals

Table 3.1 summarized the raw materials and chemicals needed for this project.

Table 3.1: List of Raw Materials and Chemicals.

Chemicals	Brand	Purpose
Zeolite	UTAR	Raw material
Distilled water H_2O	UTAR	To dissolve chloride salt
Sodium chloride NaCl	UTAR	Metal precursor for cation exchange
Potassium chloride KCl	UTAR	Metal precursor for cation exchange
Calcium chloride anhydrous $CaCl_2$	UTAR	Metal precursor for cation exchange
Magnesium nitrate hexahydrate $Mg(NO_3)_2$	UTAR	Metal precursor for cation exchange

3.1.2 Apparatus and Instruments

Table 3.2 summarized the apparatus and Instruments used in this project and their purposes.

Table 3.2: List of Apparatus and Instruments.

Apparatus and Instruments	Specification	Purpose
Analytical balance	-	To measure the mass of material
Tube Furnace Horizontal	Lenton, UK LTF 12/100/940/ 3216CC	To activate and remove impurities in the adsorbent
Hot Plate Stirrer	IKA RH basic 2	To stir and heat up solution in synthesizing the adsorbent
Thermogravimetric Analyser (TGA)	Perkin Elmer STA 8000	To measure CO_2 adsorption
X-ray Diffractometer (XRD)	Shimadzu XRD-6000	To determine the crystallite structure of adsorbent
Fourier-transform infrared spectroscopy (FTIR)	Nicolet IS10	To identify types of chemical bond of synthesized zeolite
Scanning Electron Microscope - Energy Dispersive X-ray Analyzer (SEM-EDX)	Hitachi Model S-3400N	To obtain surface morphology and composition of adsorbent

3.2 Research Flow Diagram

The research flow diagram for this project was demonstrated in Figure 3.1.

<div style="border:1px solid">

Synthesizing of Adsorbent

(i) Pre-treated the zeolite using 5 M NaCl solution and left the mixture overnight under room temperature.

(ii) KCl solution was added into the mixture for cation exchange. This procedure was performed twice, each exchanged with fresh solution.

(iii) The mixture was left for three days under room temperature.

(iv) The mixture was centrifuged and washed with distilled water for for three times to remove chloride content.

(v) The mixture was dried overnight at 80 °C.

(vi) The adsorbent obtained was heated to 400 °C and held for three hours at 400 °C to activate it and remove impurities.

(vii) Another three adsorbents were prepared using the same procedures by replacing the KCl solution with NaCl, $CaCl_2$ and $Mg(NO_3)_2$ solution, respectively.

</div>

CO_2 Analysis and Properties Study of Adsorbent

(i) TGA was used to determine the CO_2 adsorption capacity and CO_2 adsorption rate of MOR zeolite at different temperatures and after cation exchanged.

(ii) The kinetics study of CO_2 adsorption of R-MOR zeolite at different temperatures was performed.

(iii) The CO_2/N_2 selectivity at different temperatures and cation exchanged MOR zeolites were studied.

(iv) The properties study of R-MOR zeolite and cation-exchanged MOR zeolites are conducted with the aid of XRD, FTIR and SEM-EDX.

Figure 3.1: Research Flow Diagram.

3.3   Synthesizing of Adsorbent

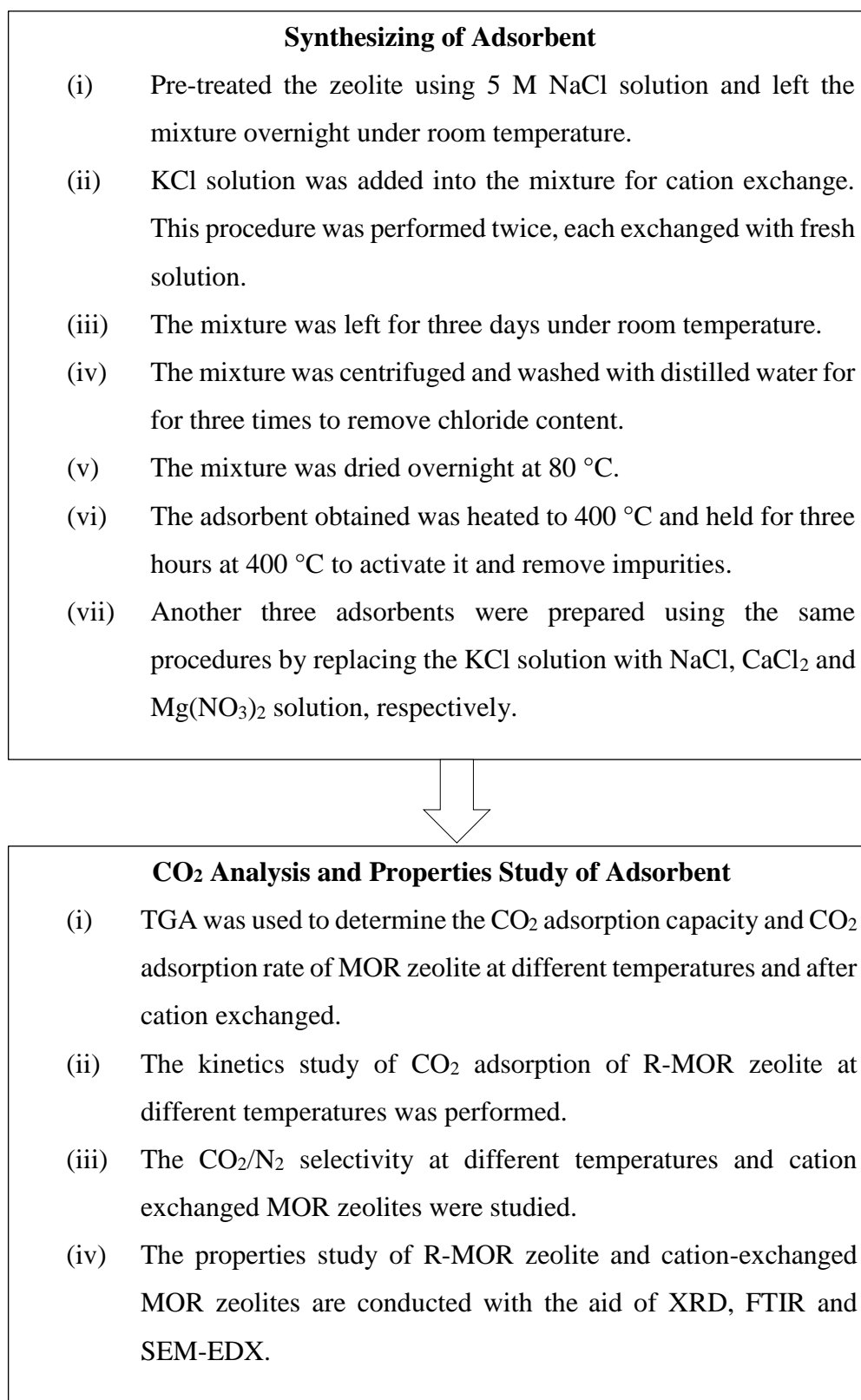The raw zeolite (adsorbent) was pre-treated with 5 M NaCl solution for 4 hours at 30 °C under constant agitation using the ratio of 20 g solid to 100 ml liquid solution. Then, the adsorbent was left overnight under room temperature.

Next, the pre-treated adsorbent was mixed with 1 M of KCl solution with ratio of 5 g solid to 50 ml liquid solution for 4 hours at 80 °C under constant agitation. The procedure was performed twice, each exchanged with fresh solution. Then, the adsorbent was left for three days under room temperature. Following that, the adsorbent was centrifuged and mixed with distilled water for 1 hour at 80 °C for three times to remove the chloride content. After that, the adsorbent was dried overnight at 80 °C to remove the water content. Lastly, the adsorbent was heated at 400 °C for 3 hours under nitrogen flow to activate it as well as to remove any impurities.

The overall procedure was repeated by replacing the KCl solution with NaCl, $CaCl_2$ and $Mg(NO_3)_2$ solution to synthesize various cation exchange zeolite. The adsorbents were denoted as raw zeolite (R-MOR), sodium exchanged zeolite (Na-MOR), potassium exchanged zeolite (K-MOR), calcium exchanged zeolite (Ca-MOR) and magnesium exchanged zeolite (Mg-MOR).

3.4 CO_2 Adsorption Capacity Measurement

The CO_2 adsorption capacity of R-MOR zeolite at 30 °C, 50 °C and 100 °C were evaluated using TGA. Prior to the measurement, the adsorbent was heated a flow of nitrogen gas, N_2 from 30 °C to 500 °C with ramping rate 20 °C/min. When the temperature reached 500 °C, the adsorbent was held for 10 min. Then, the adsorbent was allowed to cool down to the desired temperature 30 °C, 50 °C and 100 °C at 20 °C/min. An extra 30 min was set to ensure the sample temperature consistent to the programmed temperature at desired temperature. Then, the gas supplied was switched to pure carbon dioxide, CO_2. The adsorbent was held for 60 min under CO_2 flow. The mass changes of the adsorbent were recorded by TGA. The CO_2 adsorption capacity and CO_2 adsorption rate were computed using Eq. 3.1 and 3.2 with the unit of mmol/g and mmol/(g·min) respectively.

$$CO_2 \ adsorption \ capacity = \frac{(M_t - M_0) \times 1000}{M_o \times MW_{CO_2}} \qquad (3.1)$$

$$CO_2 \ adsorption \ rate = \frac{(M_t - M_0) \times 1000}{M_o \times MW_{CO_2} \times t} \qquad (3.2)$$

where

M_t = Mass of adsorbent at time t, mg

M_0 = Initial mass of adsorbent before CO_2 adsorption, mg

MW_{CO_2} = Molecular weight of CO_2, g/mol

t = Time, min

3.5 CO₂ Adsorption Kinetics Study

The kinetic study of CO_2 transport mechanism on the adsorbent can be scrutinised by the means of three developed kinetic adsorption models, namely pseudo-first order, pseudo-second order and intra-particle diffusion. The equation for pseudo-first order model, pseudo-second order model and intra-particle diffusion model were given in Eq. 3.3, Eq. 3.4 and Eq. 3.5 respectively (Gunawan, Wijiyantia, and Widiastuti, 2018).

$$\ln(q_e - q_t) = \ln q_e - kt \qquad (3.3)$$

$$\frac{t}{q_t} = \frac{1}{k_s q_e{}^2} + \frac{1}{q_e} t \qquad (3.4)$$

$$q_t = k_{id} t^{\frac{1}{2}} + C \qquad (3.5)$$

where

q_e = CO_2 adsorption capacity at equilibrium, mmol/g

q_t = CO_2 adsorption capacity at time of t, mmol/g

k = Rate constant of pseudo-first order, min^{-1}

t = Time, min

k_s = Rate constant of pseudo-second order, mmol/g

k_{id} = Diffusion constant of intra-particle diffusion, mmol/(g·min$^{-0.5}$)

C = Thickness of boundary layer

3.6   X-ray Diffraction (XRD)

The function of XRD was to characterize the crystalline structure of zeolites. Shimadzu XRD-6000 was operated at 40 kV and 30 mA under room temperature with Cu-Kα radiation of 1.5406 Å. The X-ray diffractogram was collected in 2θ range between 5° to 50° with sweep rate of 2°/min. The phase formation of zeolites can be confirmed through the comparison between diffract-grams of samples and the standard reference of zeolite. The crystallite size was calculated using Debye-Scherrer's equation in Eq. 3.6.

$$d_x = \frac{0.94\lambda}{FWHM \cdot cos\theta} \quad\quad (3.6)$$

where

d_x = Crystallite size, nm

λ = Wavelength of X−ray, (CuKα =0.15406nm)

$FWHM$ = Full width at half maximum, rad

θ = Bragg angle, rad

3.7   Fourier-transform infrared spectroscopy (FTIR)

FTIR was used to identify the types of chemical bond (functional group) in the zeolites. The FTIR analysis utilized attenuated total reflection (ATR) technique. The IR spectra of samples were compared with other relevant journal's IR spectra.

3.8   Scanning Electron Microscope - Energy Dispersive X-ray Analyzer (SEM-EDX)

SEM-EDX was used to study the morphology and composition of zeolites. Before run the analysis, the samples were coated with a thin layer of gold using Emitech SC7620 Sputter Coater to enhance the conductivity of adsorbent and increase visibility of the morphologies. EDX was connected to SEM to identify the weight and atomic percentage of different elements in the samples at five different spots.

CHAPTER 4

RESULTS AND DISCUSSION

4.1.1 Capacity and Rate of CO_2 Adsorption at Different Temperatures

To study the effect of temperature on the CO_2 adsorption capacity on R-MOR zeolite, TGA was used to determine its CO_2 adsorption capacity at 30 ℃, 50 ℃ and 100 ℃. The raw data obtained from TGA can be seen in appendix A.

The measurement results of CO_2 adsorption capacity on R-MOR zeolite at different temperatures were showed in Table 4.1 and Figure 4.1. The sample calculation of CO_2 adsorption process for R-MOR zeolite at 30 ℃ was showed in Appendix B. The CO_2 adsorption capacity of R-MOR zeolite decreased with an increase of temperature. The maximum CO_2 adsorption capacity of R-MOR zeolite was 0.1198 mmol/g at 30 ℃, followed 0.1133 mmol/g at 50 ℃ and 0.0320 mmol/g at 100 ℃. The rate of CO_2 adsorption for R-MOR zeolite at different temperatures also reduced with increase in temperature as listed in Table 4.1. Theoretically, the diffusion rate of CO_2 on R-MOR would increase with a rise of temperature because of the increase in internal energy for CO_2 at high temperature. Indeed, the high internal energy or mobility of CO_2 could reduce the restraining or trapping of CO_2 by fixed energy adsorption sites on the R-MOR surface (Hauchhum and Mahanta, 2014) and resulting in low adsorption capacity.

Since, the CO_2 adsorption of R-MOR zeolite preferred a lower temperature, the following CO_2 adsorption analysis of cation-exchanged MOR zeolite will be carried out under 30 ℃.

Table 4.1: Maximum and Average CO_2 Adsorption Capacity and CO_2 Adsorption Rate for R-MOR Zeolite at Different Temperatures.

Temperat -ure	Maximum CO_2 adsorption capacity (mmol/g)	Average CO_2 adsorption capacity (mmol/g)	Maximum CO_2 adsorption rate (mmol/g·min)	Average CO_2 adsorption rate (mmol/g·min)
30 ºC	0.1198	0.0959	0.0020	0.0016
50 ºC	0.1133	0.0696	0.0019	0.0012
100 ºC	0.0320	0.0217	0.0005	0.0004
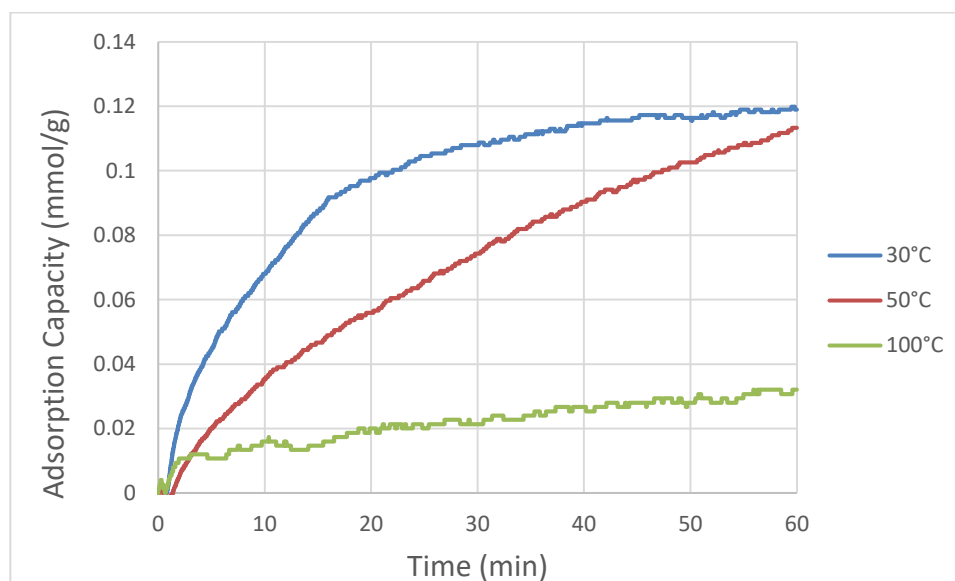
Figure 4.1: CO_2 Adsorption Capacity for R-MOR Zeolite at Adsorption Temperature of 30 °C, 50 °C and 100 °C.

4.1.2 CO_2 Adsorption Kinetic Study at Different Temperatures

To explain the mechanism of CO_2 adsorption on R-MOR zeolite, three different kinetic models were used to match the experimental data and study the mass transport process. First kinetic model was the pseudo-diffusion order model with an equation showed in Eq. 3.3. An assumption was made for this model, where the concentration of CO_2 is higher than concentration of another reactants (Gunawan, Wijiyantia, and Widiastuti, 2018). The plot of pseudo-first order was illustrated in Figure 4.2.
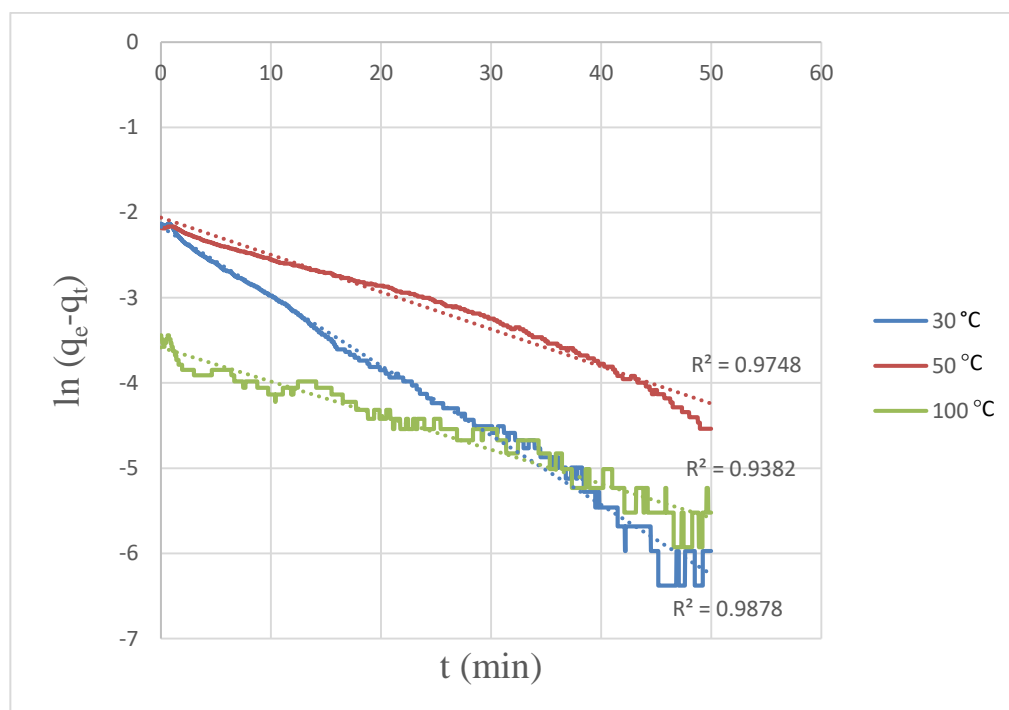
Figure 4.2: Graph of Pseudo-First Order.

Second model was the pseudo-second order model with an equation showed in Eq. 3.4. The assumption made for this model was the proportional relationship between availability of active sites on surface of R-MOR and its CO_2 adsorption capacity (Gunawan, Wijiyantia, and Widiastuti, 2018). The plot of pseudo-second order was illustrated in Figure 4.3.
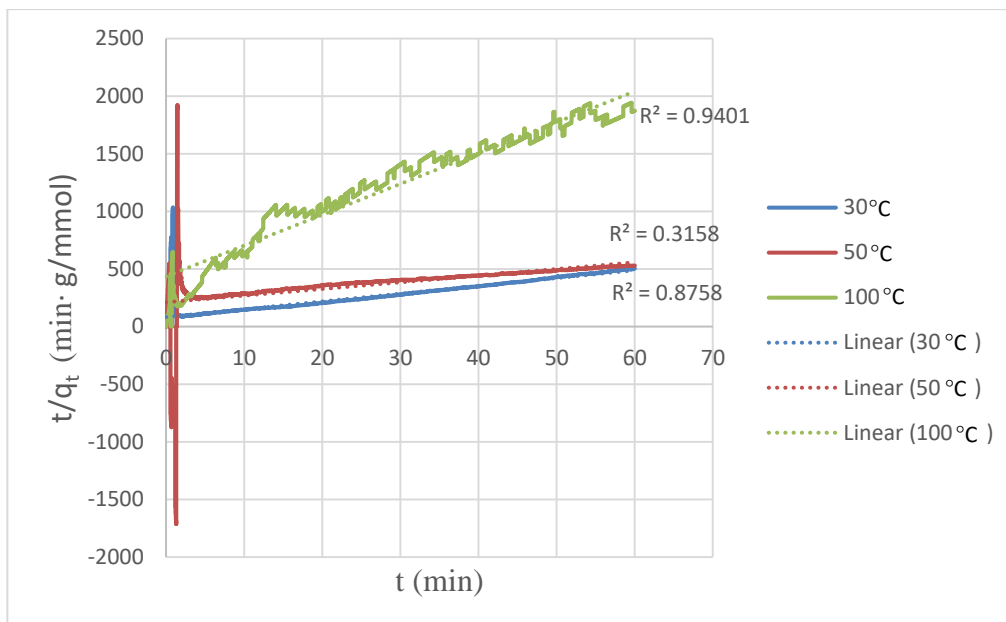
Figure 4.3: Graph of Pseudo-Second Order.

Third model was the intra-particle diffusion model with an equation showed in Eq. 3.5. In this model, two adsorption steps were introduced if the data exhibited a multi-linear plots. First step was a fast external surface diffusion, also known as macropore diffusion. Second step was a slow internal surface diffusion or micropore diffusion. The plot of intra-particle diffusion was illustrated in Figure 4.4.
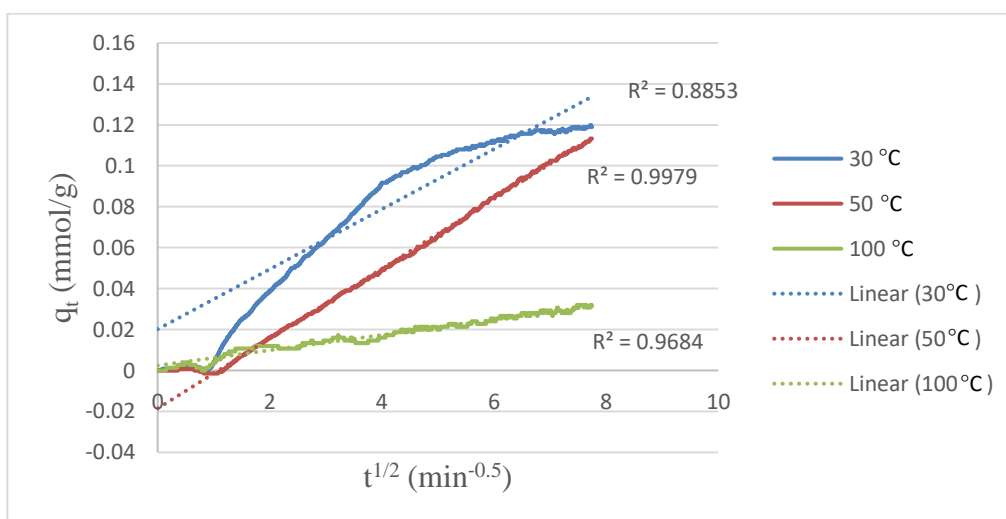
Figure 4.4: Graph of Intra-Particle Diffusion.

Table 4.2 summarized the parameters for pseudo-first order model, pseudo-second order model and intra-particle diffusion model. The kinetic data indicated that CO_2 adsorption at 30 °C followed pseudo-first order model as it gave the biggest R^2 value in agreement with Soetardji, et al (2015). The rate constant, k of pseudo-first order and pseudo-second order was a time scaling factors that related to how fast the system reaches an equilibrium. It also was a function of temperature. As the temperature of system increased, the value of rate constant in both models would decrease. The time required for the system to reach the equilibrium state would be longer at high temperature. Hence, the pseudo-first order model was used to describe the initial phase and the adsorption progress at 30 °C only. While, intra-particle diffusion is the rate-controlling for CO_2 adsorption at 50 °C and 100 °C as the values of R^2 were the biggest under this model. It was assumed that CO_2 would enter R-MOR zeolite via two steps at 50 °C and 100 °C. First was a fast external diffusion through mesopores, followed by a slow internal diffusion into micropores of R-MOR zeolite.

Table 4.2: Parameters for Each Kinetic Model.

Kinetic Model	Parameters		
Pseudo-First Order	k	q_e	R^2
30 °C	0.0816	0.1147	0.9878
50 °C	0.0437	0.1276	0.9748
100 °C	0.0400	0.0278	0.9382
Pseudo-Second Order	q_e	$k_s q_e^2$	R^2
30 °C	0.1479	0.0121	0.8758
50 °C	0.1733	4.740×10^{-3}	0.3158
100 °C	0.0374	2.299×10^{-3}	0.9401
Intra-Particle Difusion	k_{id}	C	R^2
30 °C	0.0147	0.0201	0.8853
50 °C	0.0171	-0.0185	0.9979
100 °C	0.0037	0.0024	0.9684

4.1.3 Capacity and Rate of CO_2 Adsorption after Cation Exchanged

The result in Figure 4.5 and Table 4.3 showed that the adsorption capacity of adsorbent was improved after the cation exchange. The maximum CO_2 adsorption capacity and maximum CO_2 adsorption rate of the adsorbents followed trend: Ca-MOR> Mg-MOR > Na-MOR > K-MOR > R-MOR. However, the average CO_2 adsorption capacity and average CO_2 adsorption rate of K-MOR zeolite were greater than Na-MOR zeolite within the 60 minutes. It can be related to the basic properties of adsorbent generated by the different electron densities of the framework oxygen, such that an increase in electropositivity of exchangeable cations can increase the basic strength of these sites. For instance, the basic strength of cationic zeolite containing Group 1A elements increased when $Li^+ < Na^+ < K^+ < Rb^+ < Cs^+$ as reported in Bonenfant, et al. (2008). Sometime, the basicity of adsorbent would also increase in the order of $K^+ < Na^+ < Ca^{2+}$ when the contact time between CO_2 and adsorbent was long enough as reported in Aguilar-Armenta, et al. (2001). Hence, it was reasonable that the more basic K-MOR zeolite exhibited a greater CO_2 adsorption capacity and CO_2 adsorption rate than Na-MOR zeolite at low CO_2-adsorbent contact time.
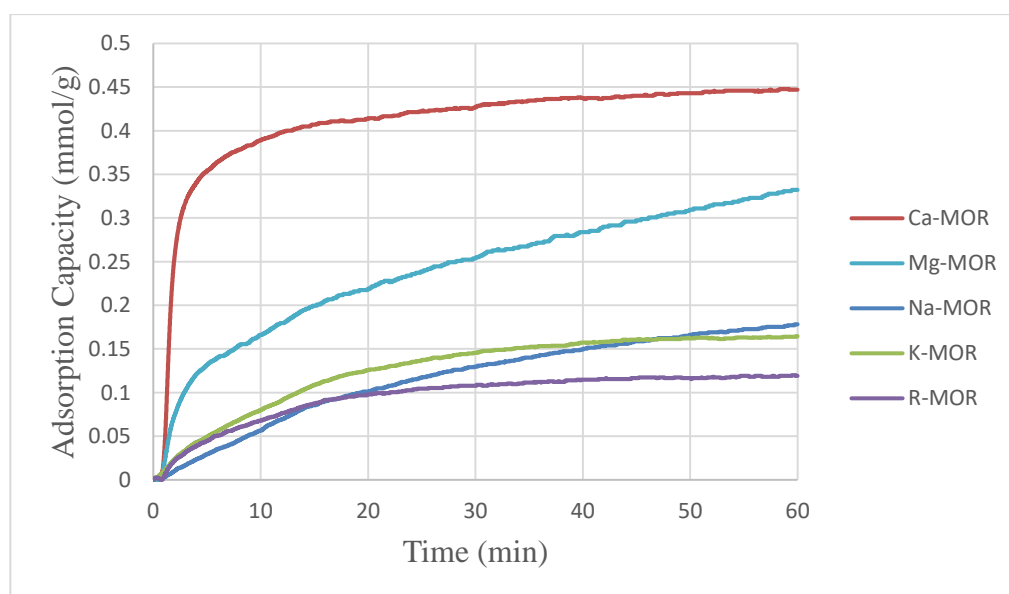

Figure 4.5: CO_2 Adsorption Capacity for R-MOR Zeolite and Cation Exchanged MOR Zeolites at Adsorption Temperature of 30 °C.

Table 4.3: Maximum and Average CO_2 Adsorption Capacity and CO_2 Adsorption Rate for Each Adsorbent at 30 °C.

Adsorbent	Maximum CO_2 adsorption capacity (mmol/g)	Average CO_2 adsorption capacity (mmol/g)	Maximum CO_2 adsorption rate (mmol/g·min)	Average CO_2 adsorption rate (mmol/g·min)
Ca-MOR	0.4478	0.4076	0.0075	0.0068
Mg-MOR	0.3323	0.2392	0.0055	0.0040
Na-MOR	0.1782	0.1163	0.0030	0.0019
K-MOR	0.1647	0.1272	0.0027	0.0021
R-MOR	0.1198	0.0959	0.0020	0.0016

The greatest CO_2 adsorption capacity in Ca-MOR zeolite might due to the occlusion of alkaline earth oxide in the adsorbent. The occlusion of oxides of calcium could increase the basicity and CO_2 adsorption capacity of the adsorbent. On the other, the basicity of the framework oxygen acting as basic center in zeolite increased when the Na^+ and K^+ were replaced by Ca^{2+} as reported in (Aguilar-Armenta, et al, 2001). In addition, the lower Si/Al ratio of Mg-MOR and Ca-MOR than K-MOR and Na-MOR also influenced the CO_2 adsorption capacity of MOR zeolite as mentioned in the discussion of EDX result under subsection 4.2.3.

The polarizing power of exchangeable cations also influenced the CO_2 adsorption capacity of adsorbent. Generally, the polarizing power of cation was inversely proportional to its ionic radius. The polarity of cations increased with the decrease of ionic radius in order of K^+ (2.20 Å) > $Na^+ \approx Ca^{2+}$ (1.80 Å) > Mg^{2+} (1.50 Å) (Crystal Maker Software, 2018). The smaller size and more polar cations such as Ca^{2+} and Mg^{2+} can penetrate more easily within the framework of adsorbent and interact more strongly with CO_2. It was noted that the CO_2 adsorption capacity of Mg-MOR zeolite was much lower than Ca-MOR zeolite which might due to low exchanged form of the adsorbent, referred to Table 4.9 under subsection 4.2.3. Some studies mentioned that the magnesium was present as $Mg(OH)_2$ instead of a free solvated cation during the cation exchange leading to the low degree of cation exchanged (Brea, et al., 2019), (Zhang, Singh

and Webley, 2008). In view of higher polarity and basic property of Mg-MOR zeolite, it was possible that the CO_2 adsorption capacity of Mg-MOR zeolite would surpass that of Ca-MOR zeolite if a fully exchanged form of adsorbent can be obtained as suggested in (Bae, 2013).

4.1.4   Selectivity of CO_2/N_2 during CO_2 Adsorption Process

Prior to measure CO_2 adsorption measurement, the adsorbents was heated from 30 °C to 500 °C under flow of nitrogen gas (N_2) to remove impurities inside the zeolite framework and reactivate it. The adsorbent was held at 500 °C for an extra 10 minutes to allow the sample temperature parallel with the programmed temperature. Then, the adsorbent was cooled down to the desired temperature. Another addition 30 min was set to ensure the sample temperature consistent to the programmed temperature at desired temperature. It was noted that N_2 was adsorbed by the adsorbent along the cooling process. The adsorption of N_2 at this stage would affect the later CO_2 adsorption process as shown in Figure A-1 to Figure A-7 in Appendix A. Then, the purging of N_2 switched to CO_2 to initiate the CO_2 adsorption process for 60 min.

The CO_2 adsorption capacity of the adsorbent was much lesser than an expected result mentioned in Figure 2.5 under subsection 2.4. This undesired result was caused by the adsorption of N_2 during the cooling stage of adsorbent in pre-treatment process. Figure 4.6 showed the weight change percent of R-MOR zeolite in pre-treatment process. The reduction of weight change occurred around 35 minutes due to the adsorption of N_2 into R-MOR zeolite. The longer time required to cool R-MOR zeolite to the desire temperature would increase the amount of N_2 adsorption as showed in Table 4.4. The lowest N_2 adsorption capacity by R-MOR zeolite was at 100 °C. To reaffirm the optimum CO_2 adsorption temperature of R-MOR zeolite, the selectivity of CO_2/N_2 was computed and tabulated in Table 4.5. Although the adsorption of N_2 at 30 °C was higher than at 100 °C, the highest CO_2/N_2 selectivity of R-MOR zeolite was at 30 °C.   This can be attributed to mobility and polarizability of CO_2. Since the polarizability and quadrupole moment of CO_2 was greater than N_2 (referred to Table 2.3 under subsection 2.4), the cation on surface framework of adsorbent would desorb the N_2 and adsorb CO_2 once the supply gas was switched. However, the increase in mobility of CO_2 at higher temperature that reduce the

retaining or capturing chances of CO_2 by R-MOR zeolite. Thus, it can be concluded that R-MOR zeolite exhibited highest CO_2 adsorption capacity and selectivity of CO_2/N_2 at 30 °C. The sample calculation for N_2 adsorption capacity and CO_2/N_2 selectivity were showed in Appendix B.

Figure 4.6: Weight Change Percent for R-MOR Zeolite at Pre-treatment Stage.

Table 4.4: Maximum and Average N_2 Adsorption Capacity and CO_2/N_2 Selectivity for R-MOR Zeolite during Cooling Process of Pre-treatment to Desired Temperatures.

Desired Temperature	Maximum N_2 adsorption capacity (mmol/g)	Average N_2 adsorption capacity (mmol/g)	Maximum CO_2/N_2 Selectivity	Average CO_2/N_2 Selectivity
30 ºC	1.0201	0.5730	0.1175	0.1673
50 ºC	1.4355	0.7973	0.0789	0.0873
100 ºC	0.6159	0.2897	0.0520	0.0749

Following that, the weight change and CO_2/N_2 selectivity of the each cation exchanged adsorbent at 30 °C were illustrated in Figure 4.7 and tabulated in Table 4.5. The N_2 adsorption of the adsorbents decreased as Na-MOR> R-MOR> Mg-MOR> Ca-MOR, whereas the CO_2/N_2 selectivity increased as Na-

MOR < R-MOR< Mg-MOR< Ca-MOR. These results can be correlated to the polarizing power of exchangeable cation as mentioned in subsection 4.1.3 and quadrupole moment of the adsorbates. The smaller exchangeable cation with higher polarizing power would attract the more quadrupole moment adsorbate, CO_2. Although the data of K-MOR zeolite had been omitted in this project, the, it was expected that K-MOR zeolite would exhibit lower N_2 adsorption and higher CO_2/N_2 selectivity than Na-MOR zeolite with reference result obtained by Dangi, et al. (2012).

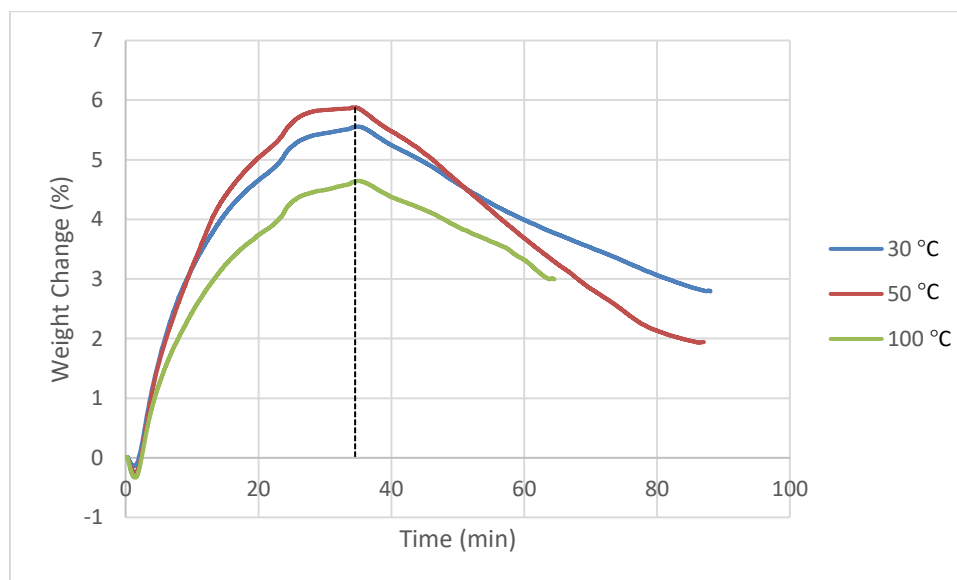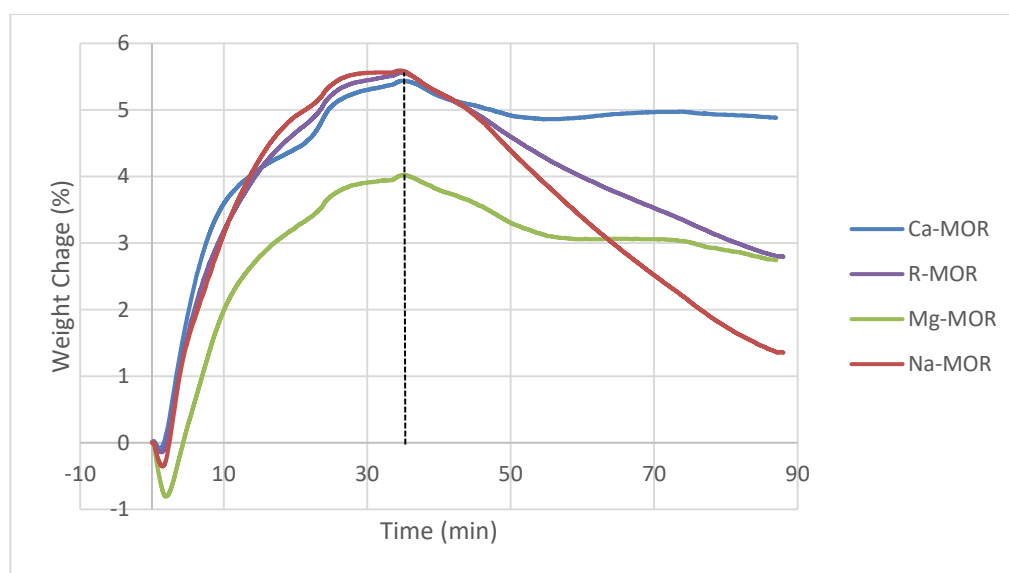
Figure 4.7: Weight Change Percent for Each Adsorbent at Pre-treatment Stage.

Table 4.5: Maximum and Average N_2 Adsorption Capacity and CO_2/N_2 Selectivity for Each Adsorbent during Cooling Process of Pre-treatment to 30 °C.

Adsorbent	Maximum N_2 adsorption capacity (mmol/g)	Average N_2 adsorption capacity (mmol/g)	Maximum CO_2/N_2 Selectivity	Average CO_2/N_2 Selectivity
Ca-MOR	0.2168	0.1684	2.0655	2.4203
Mg-MOR	0.4736	0.3010	0.7015	0.7947
Na-MOR	1.5991	0.8442	0.1114	0.1378
R-MOR	1.0201	0.5730	0.1175	0.1673

4.2   Characterisation of Adsorbent

4.2.1   X-ray Diffraction (XRD)

XRD technique was used to determine the crystal structure and identify crystallite phase of the adsorbents. The XRD diffractograms for all adsorbents that displayed in Figure 4.8 were consistent with the characteristic peaks of mordenite-type zeolite in Mintova and Barrier (2016), where the peaks were almost at 2θ: 9°, 22°, 25° and 27°. The label 'M' represented mordenite components. Thus, the adsorbents used in this experiment was probably a mordenite type zeolite, in conjugation with the SEM-EDX result.
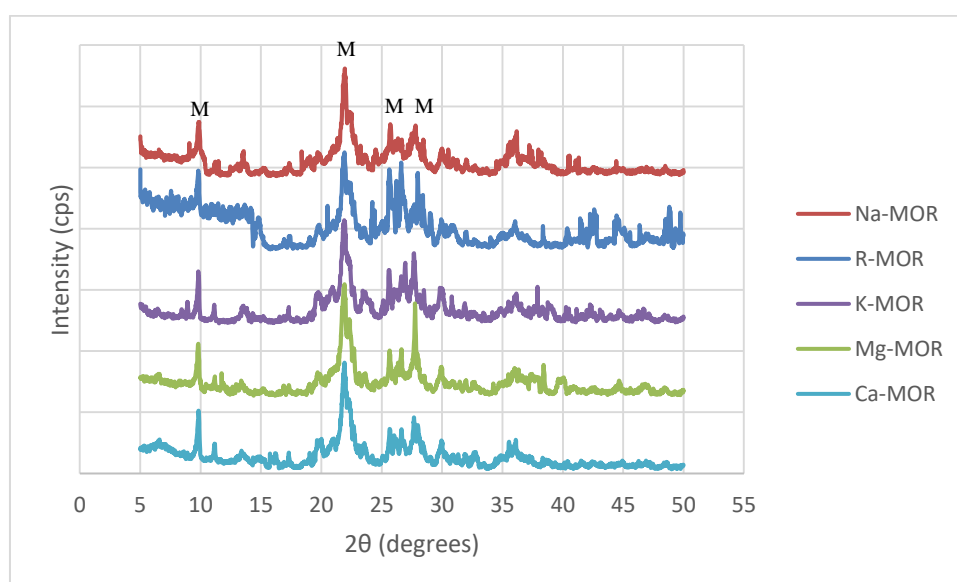
Figure 4.8: XRD Patterns for MOR Zeolite.

In general, the modification of R-MOR zeolite through cation-exchange did not lead to distinct structural changes of the samples. This indicated the cation-exchange did not destroy or change the framework of zeolite. Nevertheless, the intensity of the characteristic peaks that attributed to framework cations decreased considerably for Na-MOR zeolite, K-MOR zeolite, Mg-MOR zeolite and Ca-MOR zeolite, except for an increased intensity of peak around 27° in Mg-MOR zeolite. The change in intensity of these peaks were due to the compositional change within the mineral after the cation exchange.

The three strongest peaks of each adsorbent listed in Table 4.6 indicated that the minerals were appropriate with mordenite zeolite. The crystallite size of

each adsorbent was computed by using Debye-Scherrer equation and a sample calculation was showed in Appendix C. The average crystallite size of the adsorbent was decreased after cation exchange with potassium and magnesium; increased after the cation-exchange with sodium and calcium. In order to have a clearer picture about the crystallize size of the adsorbents, the actual crystal size image of the adsorbents were provided under SEM-EDX subsection.

Table 4.6: The Three Strongest XRD Peaks for Each Adsorbent.

Adsorbent	Peak No.	2θ (deg)	2θ (rad)	Full Width at Half Maximum (deg)	Full Width at Half Maximum (rad)	Crystallite Size (nm)	Average Crystallite Size (nm)
R-MOR	12	22.0693	0.385182	1.0763	0.018785	7.854374	
	15	25.7391	0.449232	0.6917	0.012072	12.30472	**10.76788**
	16	26.6360	0.464886	0.7021	0.012254	12.14454	
K-MOR	13	21.9701	0.383451	0.8438	0.014727	10.01688	
	18	27.6544	0.482660	0.6054	0.010566	14.11463	**10.41242**
	17	26.6500	0.465130	1.2000	0.020944	7.105773	
Na-MOR	13	22.0561	0.384952	0.8448	0.014745	10.00648	
	4	9.82620	0.17150	0.4390	0.007662	18.97031	**12.7442**
	18	27.6527	0.482631	0.9232	0.016113	9.255809	
Ca-MOR	11	22.0252	0.384412	0.8448	0.014745	10.00595	
	16	27.8414	0.485924	0.4390	0.007662	19.47253	**12.83297**
	2	9.7774	0.170648	0.9232	0.016113	9.020433	
Mg-MOR	11	22.0217	0.384351	1.0099	0.017626	8.370115	
	16	27.7333	0.484037	0.6400	0.011170	13.35382	**10.48878**
	15	26.5175	0.462818	0.8750	0.015272	9.742398	

4.2.2   Fourier-transform infrared spectroscopy (FTIR)

FTIR technique is used to determine the function group of the adsorbents before and after CO_2 adsorption. Figure 4.9 showed the structure of zeolite changed slightly after cation exchanged. The fundamental IR spectra for the adsorbents were in the range of 400 cm^{-1} to 3800 cm^{-1}.
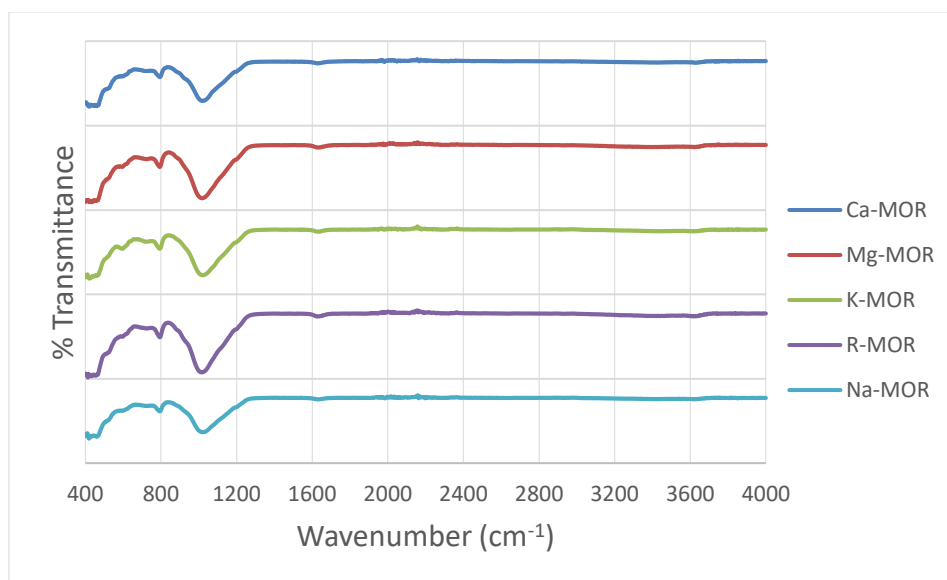
Figure 4.9: FTIR Spectra for Each Adsorbent before CO_2 Adsorption.

All adsorbents showed the essential peaks for zeolite material such as the hydroxyl-silanol group vibration stretch (Si-OH) in between 3618.23 cm^{-1} to 3627.83cm^{-1}. The peaks around 794.28-793.13 cm^{-1} and 1022.95-1015.74 cm^{-1} showed the existence of symmetric and asymmetric O-T-O vibration, $v_{(O-T-O)}$ stretch of external linkages in zeolite framework as suggested in Li (2005). The term 'T' can be Si or Al. The IR peaks at 595.42 cm^{-1}, 424.43 cm^{-1} and 420.36 cm^{-1} represented the T-O bend.

The position and intensity of the peaks in R-MOR zeolite were slightly changed after the introduction of exchangeable cations, especially the broad peak centred on 1015.74 cm^{-1}. The shifting of peaks in R-MOR zeolite after cation exchanged suggested that the presence of zeolite external structural vibrations due to possible loss of Al atoms or change in bonding capacity and angle of Si-O-Si (Syukri, et al., 2019).

According to Stevens, Siriwardane and Logan (2008), different modes of carbonate would appear in between 980 cm^{-1} and 1630 cm^{-1} after the adsorption of CO_2 as showed in Figure 4.10. From Table 4.7 and Table 4.8, it is noted that all adsorbents had peaks round 1627.89 cm^{-1} and 1633.91 cm^{-1} which were the bridged bidentate carbonate. This indicated that the adsorbent can adsorb CO_2 in room temperature as well as a raise of temperature till 100 °C. However, the CO_2 adsorption capacity reduces as the temperature increases, where the peaks of bridged bidentate carbonate at 1633.91 cm^{-1} showed a slight shift and intensity increase with a rise of temperature as shown in Appendix D. Based on the literature in Galhotra (2010), a physisorbed peaks of CO_2 can be detected around 2350 cm^{-1} through an *in situ* FTIR investigation. However, the physisorbed peaks of CO_2 were undetected here for the adsorbents after the purging of CO_2 at different temperatures because the *in situ* analysis of TGA-FTIR analysis was not applied.
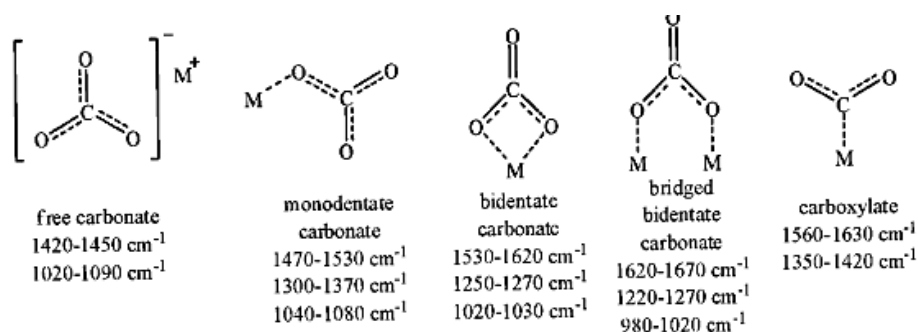
Figure 4.10: Different Modes of Carbonate Formed after CO_2 Adsorption (Stevens, Siriwardane and Logan, 2008).

Table 4.7: IR Spectra Peaks for Each Adsorbent before CO_2 Adsorption.

Adsorbent	IR Spectra Peaks (cm^{-1})				
R-MOR	3618.23	-	1633.89	1015.74	794.28	-
K-MOR	3627.83	-	1633.80	1020.06	793.13	595.42/ 424.43
Na-MOR	3622.27	2163.38/ 2050.81	1628.24	1022.95	793.57	-
Mg-MOR	3625.11		1635.49	1019.59	793.34	-
Ca-MOR	3621.25	1980.28	1628.76	1019.21	794.16	420.36

Table 4.8: IR Spectra Peaks for Each Adsorbent after CO_2 Adsorption at 30 °C.

Adsorbent	IR Spectra Peaks (cm^{-1})					
R-MOR	3391.31		1633.91	1015.55	793.97	
K-MOR	3733.76/	2323.06/	1633.85	1035.83	792.14	598.10/
	3627.18	2177.72/				4724.04/
		2161.58/				463.85/
Na-MOR	3289.95	-	1627.97	1019.01	793.88	421.46
Mg-MOR	3378.92	-	1632.99	1012.08	792.72	-
Ca-MOR	3600.57	2068.98/	1628.66	1030.30	793.26	420.36
		2169.82/				
		2195.95				

4.2.3 Scanning Electron Microscope - Energy Dispersive X-ray Analyzer (SEM-EDX)

SEM was used to study the surface morphology of the adsorbents while EDX was used to determine the surface composition. The SEM images for the adsorbents were showed in Figure 4.11.

(a)

(b)

(c)

(d)

(e)

Figure 4.11: SEM Images of (a) R-MOR; (b) K-MOR; (c) Na-MOR; (d) Ca-MOR; (e) Mg-MOR after Calcined to 400 °C.

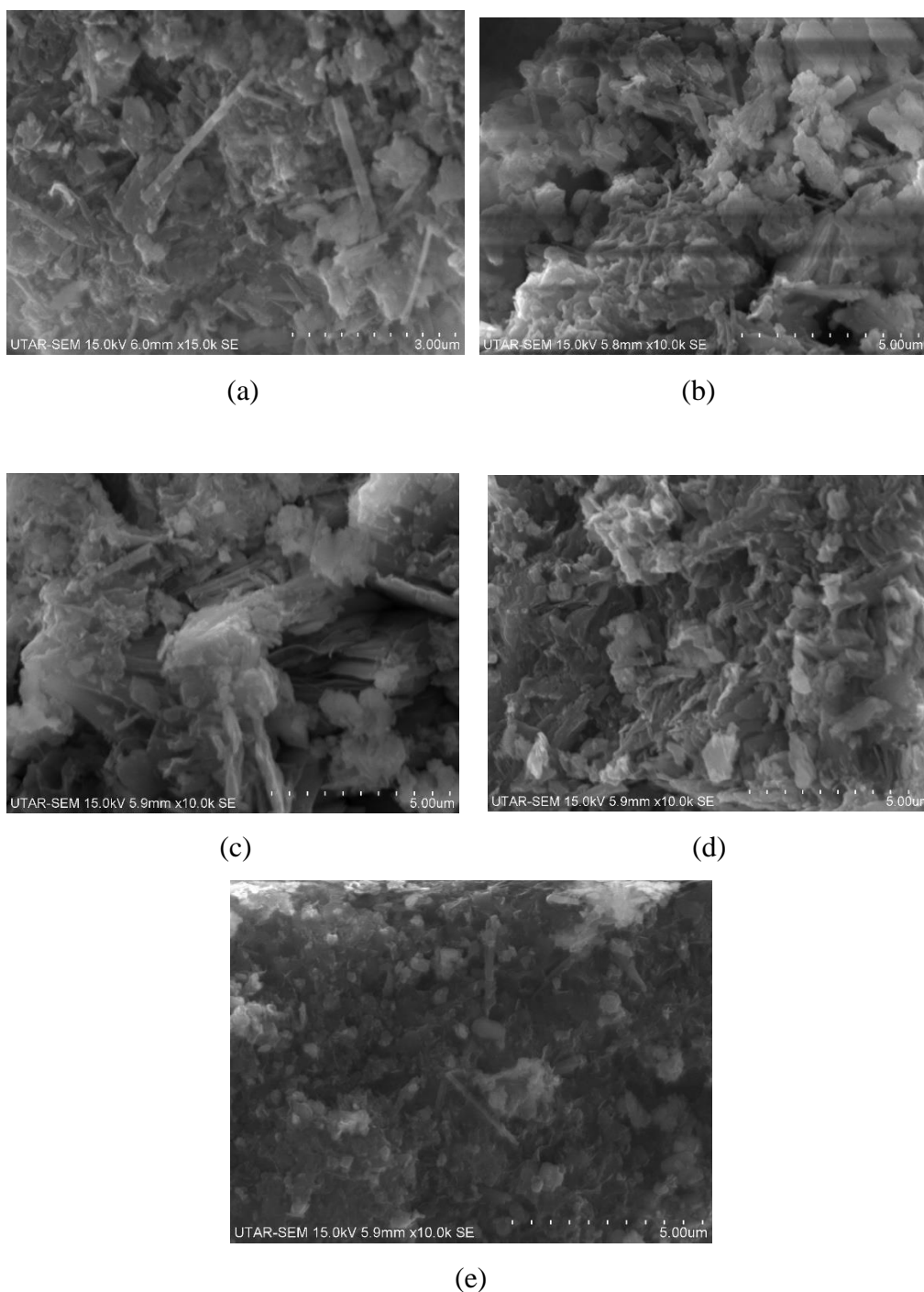The SEM images showed the surface morphology of the adsorbents had no significant changes after cation exchange. The structures can be described as nanofiber-like crystal and some amorphous globules made of entangled zeolite fibres. The attribution of less uniform structure around nanofiber-like shape of zeolite structure was caused by mechanical force during grinding the zeolite (Soetardji, et al, 2015). The crystalline structure of the adsorbents were consistent with the XRD results.

The EDX results for each adsorbent were listed in Appendix E. It was noted that the distribution of elements on each tested areas varies at five spots of the adsorbents. From Table 4.9, it showed that the exchange capacity of cations of adsorbent were below the maximum exchange capacity. Although the R-MOR zeolite was cation-exchanged with other cations such as K^+, Na^+, Ca^{2+}, and Mg^{2+}, the value of K/Al ratio was the greatest among ratios: K/Al, Ca/Al, Na/Al, and Mg/Al. This indicated that the adsorbent had better affinity towards K^+, which in agreement with result obtained in Villarreal, Castillo-Villalon, and Ramirez (2017) that stated that the low cation exchange capacity in adsorbent was probably caused by low mobility of cations in the side pockets.

Table 4.9: Atomic Ratio for Each Adsorbent Based on EDX Result.

Adsorbent	Average Ratio				
	K/ Al	Na/Al	Ca/ Al	Mg/ Al	Si/Al
R-MOR	0.2435	0.1224	0.1041	-	4.945
Na-MOR	0.2275	0.3532	0.0831	-	5.809
K-MOR	0.5945	0.1139	0.0562	-	5.479
Ca-MOR	0.2149	0.0783	0.2742	-	5.3384
Mg-MOR	0.2052	0.1556	0.0614	0.1416	4.9227

Regarding the Si/ Al ratio, all adsorbents had the ratio around 5 except for Na-MOR zeolite, 5.809 which is slightly higher. This may due to dealumination effect in Na-MOR zeolite when cation exchange the RZ with NaCl in batch. Nevertheless, the adsorbents were classified under mordenite-type zeolite as the typical Si/Al ratio of mordenite zeolite was 5 (Mohammad Hassnaian, 2017). It was noted that the Si/Al ratio of Mg-MOR zeolite and Ca-MOR zeolite were

considerably lower than K-MOR zeolite and Na-MOR zeolite. The lower Si/Al ratio would has better CO_2 adsorption capacity at low temperature with the support of TGA result under subsection 4.1.3. At low Si/Al ratio, the presence of more Al-atoms in framework increased the number of charged sites and the surface basicity of adsorbent, which attributed stronger attraction between acidic CO_2 and adsorbent.

In accordance with the XRD diffractograms, SEM images and Si/Al ratio of the adsorbents, it can be concluded that the adsorbents were the mordenite-type zeolite.

CHAPTER 5

CONCLUSIONS AND RECOMMENDATIONS

5.1 Conclusions

The optimum adsorption temperature for MOR zeolite was at 30 °C. At 30 °C, R-MOR zeolite exhibited the best performance in CO_2 adsorption process with the maximum CO_2 adsorption capacity and maximum CO_2 adsorption rate of 0.1198 mmol/g and 0.0020 mmol/(g·min) respectively. R-MOR zeolite also showed the highest maximum CO_2/N_2 selectivity at 30 °C. The mass transport mechanism of CO_2 adsorption at 30 °C followed pseudo-first order model with R^2 value of 0.9878, at 50 °C and 100 °C followed intra-particle diffusion with R^2 value of 0.9979 and 0.9684 respectively. The CO_2 adsorption of cation exchanged MOR zeolite was performed at 30 °C, the results showed the maximum CO_2 adsorption capacity and maximum CO_2 adsorption rate followed trend: Ca-MOR> Mg-MOR > Na-MOR > K-MOR > R-MOR within 60 minutes. Among the cation exchanged adsorbents, Ca-MOR zeolite had the highest maximum CO_2/N_2 selectivity. Based on the XRD result, the adsorbents showed the characteristic peaks of mordenite-type zeolite and the intensity of peaks were decreased as a result of compositional change within the mineral after the cation exchange. The FTIR result showed the function groups of MOR zeolite and the peak for CO_2 adsorbed on the adsorbents. The SEM images showed the structure of the adsorbent was nanofiber-like crystal and some amorphous globules made of entangled zeolite fibres. Whereas, the EDX result indicated that the adsorbents had a better affinity towards K^+ during cation exchange.

5.2 Recommendations for future work

As mentioned in previous part, the Mg-MOR zeolite might has greater CO_2 adsorption capacity and CO_2 adsorption rate if a fully exchanged form of adsorbent can be obtained. Thus, it is recommended to study the CO_2 adsorption capacity and CO_2 adsorption rate of a fully cation exchanged adsorbent. The kinetic study for the adsorption mixture gas, CO_2-N_2 by MOR zeolite can be further studied by varying the pressure and temperature during adsorption process. Besides, the presence of water and other gaseous can be added during the CO_2 adsorption process of adsorbent.

REFERENCES

Aguilar-Armenta, G., Hernandez-Ramirez, G., Flores-Loyola, E., Ugarte-Castaneda, A., Silva-Gonzalez, R., Tabares-Munoz, C., Jimenez-Lopez, A., and Rodriguez-Castellon, E., 2001. Adsorption Kinetics of CO_2, O_2, N_2, and CH_4 in Cation-Exchanged Clinoptilolite. *The Journal of Physical Chemistry B*, 105(7), pp. 1313–1319.

Aimen Isa, M., Chew, T. L., and Yeong, Y. F., 2018. Zeolite NaY Synthesis by using Sodium Silicate and Colloidal Silica as Silica Source. *IOP Conference Series: Materials Science and Engineering*, 458, pp. 012001.

Aslı ERTAN, 2004. *CO_2, N_2 and Ar Adsorption on Zeolites*. Master. İzmir Institute of Technology. Available at: <http://library.iyte.edu.tr/tezler/master/kimyamuh/T000295.pdf> [Accessed 12 May 2020].

AZoM, 2006. *Aluminate from Basic Aluminium Sulfate*. [online] Available at: <https://www.azom.com/article.aspx?ArticleID=3517> [Accessed 20 August 2019].

Bae, T.-H., Hudson, M. R., Mason, J. A., Queen, W. L., Dutton, J. J., Sumida, K., Sumida, K., Micklash, K. J., Kaye, S. S., Brown, C. M. and Long, J. R., 2013. Evaluation of cation-exchanged zeolite adsorbents for post-combustion carbon dioxide capture. *Energy Environ. Sci.,* 6(1), pp. 128–138.

Berger, A. H. and Bhown. A. S., 2011. Comparing physisorption and chemisorption solid sorbents for use separating CO_2 from flue gas using temperature swing adsorption. *Energy Procedia*, 4, pp. 562-567.

Brandani, F. and Ruthven, D. M., 2004. The Effect of Water on the Adsorption of CO_2 and C_3H_8 on Type X Zeolites. *Ind. Chem. Res*. 43 (26), pp. 8339-8344.

Bensafi, B., Chouat, N. and Djafri, F., 2017. High performance of carbon dioxide adsorption of mesoporous mordenite synthesized in the presence of N,N-dimethylaniline. *Res Chem Intermed*, 43, pp. 7443–7456.

Berkeley Earth, 2019. *Global Temperature Report for 2017*. [online] Available at: <http://berkeleyearth.org/global-temperatures-2017/> [Accessed 24 June 2019].

Bonenfant, D., Kharoune, M., Niquette, P., Mimeault, M., and Hausler, R., 2008. Advances in principal factors influencing carbon dioxide adsorption on zeolites. *Science and technology of advanced materials*, 9(1), pp. 013007.

Brea, P., Delgado, J. A., Águeda, V. I., Gutiérrez, P., and Uguina, M. A., 2019. Multicomponent adsorption of H_2, CH_4, CO and CO_2 in zeolites NaX, CaX and MgX. Evaluation of performance in PSA cycles for hydrogen purification. *Microporous and Mesoporous Materials.* 286, pp. 187-198.

Chemical Dictionary, 2017. *Definition of Polarizability.* [online] Available at: <https://www.chemicool.com/definition/polarizability.html> [Accessed 17 March 2020].

Chemistry LibreTexts, 2019. *Quadrupolar Coupling.* [online] Available at: <https://chem.libretexts.org/Bookshelves/Physical_and_Theoretical_Chemistry_Textbook_Maps/Supplemental_Modules_(Physical_and_Theoretical_Chemistry)/Spectroscopy/Magnetic_Resonance_Spectroscopies/Nuclear_Magnetic_Resonance/NMR_-_Theory/NMR_Interactions/Quadrupolar_Coupling> [Accessed 17 March 2020].

Crystal Maker Software, 2018. *Elements, Atomic Radii and the Periodic Table.* [online] Available at: <http://www.crystalmaker.com/support/tutorials/atomic-radii/?fbclid=IwAR0B58E3aWOSf7tw6mKo8If2U7Phn0faS-wJ73xd5jGWnNuJUnMrBU2LDDs> [Assessed 11 March 2020].

Dangi, G. P., Munusamy, K., Somani, R. S., and Bajaj, Hari. C., 2012. Adsorption selectivity of CO_2 over N_2 by cation exchanged zeolite L: Experimental and simulation studies. *Indian Journal of Chemistry*, Section a. 51A. pp. 1238-1251.

Díaz, E., Muñoz, E., Vega, A., and Ordóñez, S., 2008. Enhancement of the CO_2 Retention Capacity of Y Zeolites by Na and Cs Treatments: Effect of Adsorption Temperature and Water Treatment. *Ind. Eng. Chem. Res, 47*(2), pp. 412-418.

Dunstan, M., Jain, A., Liu, W., Ong, S., Liu, T., Lee, J., Persson, K., Scott, S., Dennis, J. and Grey, C., 2016. Large scale computational screening and experimental discovery of novel materials for high temperature CO_2 capture. *Energy & Environmental Science*, 9(4), pp. 1346-1360.

Grajciar, L., Čejka, J., Zukal, A., Otero Areán, C., Turnes Palomino, G., and Nachtigall, P., 2012. Controlling the Adsorption Enthalpy of CO_2 in Zeolites by Framework Topology and Composition. *ChemSusChem,* 5(10), pp. 2011–2022.

Galhotra, P., 2010. *Carbon dioxide adsorption on nanomaterials*. PhD. University of Iowa. Available at: <https://ir.uiowa.edu/cgi/viewcontent.cgi?article=1855&context=etd> [Assessed 27 March 2020].

Gunawan, T., Wijiyantia, R., and Widiastuti, N., 2018. Adsorption–desorption of CO_2 on zeolite-Y-templated carbon at various temperatures. *RSC Advances*. [e-journal] 8(72), pp. 41594-41602. Available through: Royal Society of Chemistry <https://pubs.rsc.org/en/Content/ArticleLanding/2018/RA/C8RA09200A#!divAbstract> [Assessed 17 March 2020].

Hauchhum, L., and Mahanta, P., 2014. Carbon dioxide adsorption on zeolites and activated carbon by pressure swing adsorption in a fixed bed. *Int J Energy Environ Eng*, 5, pp. 349–356.

Hisham, M. A., Moustafa. E. M. and Ehab, A. A., 2011. Influence of Aluminum Source on the Synthesis of Nanosized ZSM-5 Zeolite. *Der Chemica Sinica Pelagia Research Library*, 2(4), pp. 166-173.

Lee, S.-Y., and Park, S.-J., 2015. A review on solid adsorbents for carbon dioxide capture. *Journal of Industrial and Engineering Chemistry,* 23, pp. 1–11.

Li, G. H., 2005. *FT-IR studies of zeolite materials: characterization and environmental applications*. PhD. University of Iowa. Available at <https://ir.uiowa.edu/cgi/viewcontent.cgi?referer=https://www.google.com/&httpsredir=1&article=1281&context=etd> [Assessed 11 March 2020].

Megías-Sayago, C., Bingre, R., Huang, L., Lutzweiler, G., Wang, Q., and Louis, B., 2019. CO_2 Adsorption Capacities in Zeolites and Layered Double Hydroxide Materials. *Frontiers in chemistry*, 7, pp. 551.

Mintova, S. and Barrier, N., 2016. *Verified Syntheses of Zeolitic Materials*. 3rd ed. Normandie Université, France: Synthesis Commission of the International Zeolite Association.

Mohammad Hassnaian, 2017. *An Experimental Enquiry into Growth of Moerdenite Nanocrytals Sans Seed Addition.* Master. Edith Cowan University. Available at: < https://www.researchgate.net/publication/314282598_An_Experimental_Enquiry_into_The_Growth_of_Mordenite_Nanocrystals_Sans_Seed_Addition> [Accessed 27 March 2020].

Mohau, M, Misael, S. N., and Veronica, O., 2017. A Review of the Chemistry, Structure, Properties and Applications of Zeolites. *American Journal of Materials Science*, 7(5), pp. 196-221.

Nediljka. G. M. and Karolina. N. M., 2019. *Carbon Capture and Storage (CCS): Geological Sequestration of CO_2.* [online] Available at: <https://www.intechopen.com/online-first/carbon-capture-and-storage-ccs-geological-sequestration-of-co2> [Accessed 24 June 2019].

Petrov, I.A., and Michalev, T., 2012. Synthesis of Zeolite A: A Review. [online] Available at: <https://pdfs.semanticscholar.org/080d/64892e31cef52edac82141f8a4c6a08440ac.pdf> [Accessed 18 August 2019].

Salehi, S., and Anbia, M., 2017. Characterization of CPs/Ca-exchanged FAU- and LTA-type zeolite nanocomposites and their selectivity for CO_2 and N_2 adsorption. *Journal of Physics and Chemistry of Solids*, 110, pp. 116–128.

Soetardji, J. P., Claudia, J. C., Ju, Y.-H., Hriljac, J. A., Chen, T. Y., Soetaredjo, F. E., Santoso, S. P., Kurniawan, A., and Ismadji, S., 2015. Ammonia removal from water using sodium hydroxide modified zeolite mordenite. *RSC Advances*, 5(102), pp. 83689–83699.

Stevens, R. W., Siriwardane, R. V., and Logan, J., 2008. In Situ Fourier Transform Infrared (FTIR) Investigation of CO_2 Adsorption onto Zeolite Materials. *Energy & Fuels*, 22(5), pp. 3070–3079.

Syukri, Islami, D. M., Saputra, Y., Seprianti, S., Wahyuni, S., Ramadhani, F., Arief, S., Tetra, O. N., Putri, Y. E. and Rilda, Y., 2019. Natural Zeolits and Its Modifications with Protons and Copper as the Catalyst for Esterification of Ethanol with Acetic Acid. *KnE Engineering*, 4(2), pp. 296–306.

Villarreal, A., Castillo-Villalon, P., and Ramirez, J., 2017. Analysis of the interaction of CO_2 with Na, K, and Ca-exchanged Mordenite. An infrared spectroscopic study. *J. Mex. Chem. Soc*, [e-journal] 61(2), pp.102-108. Available through: Scielo <http://www.scielo.org.mx/scielo.php?script=sci_arttext&pid=S1870-249X2017000200102#B26> [Assessed 13 March 2020].

Walton, K. S., Abney, M. B., and Douglas LeVan, M., 2006. CO_2 adsorption in Y and X zeolites modified by alkali metal cation exchange. *Microporous and Mesoporous Materials*, 91(1-3), pp. 78–84.

Wang. Q, Luo. J., Zhong. Z. and Armando. B., 2011. CO_2 capture by solid adsorbents and their applications: current status and new trends. *Energy & Environmental Science*, 4, pp. 42-55.

Xu, G., Zhu, X., Li, X., Xie, S., Liu, S., and Xu, L., 2010. Synthesis of pure silica ITQ-13 zeolite using fumed silica as silica source. *Microporous and Mesoporous Materials*, 129(1-2), pp. 278–284.

Yamazaki, T., Katoh, M., Ozawa, S., and Ogino, Y, 1993. Adsorption of CO_2 over univalent cation-exchanged ZSM-5 zeolites. *Molecular Physics*, 80(2), pp. 313–324.

Yang, S.-T., Kim, J., and Ahn, W.-S., 2010. CO_2 adsorption over ion-exchanged zeolite beta with alkali and alkaline earth metal ions. *Microporous and Mesoporous Materials,* 135(1-3), pp. 90–94.

Younas, M., Sohail, M., Leong, L. K., Bashir, M. J., and Sumathi, S., 2016. Feasibility of CO_2 adsorption by solid adsorbents: a review on low-temperature systems. *International Journal of Environmental Science and Technology*, 13(7), pp. 1839–1860.

Zhang, J., Singh, R., and Webley, P. A., 2008. Alkali and alkaline-earth cation exchanged chabazite zeolites for adsorption based CO_2 capture. *Microporous Mesoporous Mater,* 111, pp. 478–487.

911Metallurgist, 2017. *Zeolite – Natural and Synthetic.* [online] Available at: < https://www.911metallurgist.com/zeolites/> [Accessed 18 August 2019].

APPENDICES

APPENDIX A: TGA Raw Data

The complete raw data set obtained from TGA for CO_2 adsorption was too large, consists of 6000 points because 0.01 minutes specification difference had been applied. Thus, the weight change of the adsorbent at first 0.48 minutes was tabulated in Table A-1 as a sample.

Table A-1: TGA Raw Data for CO_2 Adsorption of the Each Adsorbent at Different Temperatures.

Time (min)	Weight of Adsorbent (mg)			K-MOR	Na-MOR	Ca-MOR	Mg-MOR
	R-MOR						
	30 °C	50 °C	100 °C	30 °C	30 °C	30 °C	30 °C
0	26.739	29.69	17.036	33.247	24.487	23.846	15.045
0.01	26.74	29.69	17.036	33.247	24.487	23.846	15.045
0.02	26.74	29.69	17.036	33.248	24.488	23.846	15.045
0.03	26.74	29.69	17.037	33.248	24.488	23.846	15.045
0.04	26.74	29.69	17.037	33.248	24.488	23.846	15.045
0.05	26.74	29.69	17.037	33.248	24.488	23.846	15.045
0.06	26.74	29.69	17.037	33.248	24.488	23.846	15.045
0.07	26.74	29.69	17.037	33.248	24.488	23.847	15.045
0.08	26.74	29.69	17.037	33.248	24.488	23.847	15.045
0.09	26.74	29.69	17.037	33.248	24.488	23.847	15.045
0.1	26.74	29.69	17.037	33.249	24.488	23.847	15.045
0.11	26.74	29.69	17.037	33.249	24.488	23.847	15.045
0.12	26.74	29.69	17.037	33.249	24.489	23.846	15.045
0.13	26.741	29.69	17.038	33.249	24.489	23.846	15.045
0.14	26.741	29.691	17.038	33.249	24.489	23.846	15.045
0.15	26.741	29.691	17.038	33.249	24.489	23.846	15.045
0.16	26.741	29.691	17.038	33.249	24.489	23.846	15.045

Table A-1 (Continued)

0.17	26.741	29.691	17.038	33.249	24.489	23.846	15.045
0.18	26.741	29.691	17.038	33.25	24.489	23.846	15.045
0.19	26.741	29.691	17.038	33.25	24.489	23.846	15.045
0.2	26.741	29.691	17.038	33.25	24.489	23.846	15.045
0.21	26.741	29.691	17.038	33.25	24.49	23.846	15.045
0.22	26.741	29.691	17.038	33.25	24.49	23.846	15.045
0.23	26.741	29.691	17.038	33.25	24.49	23.846	15.045
0.24	26.741	29.691	17.039	33.25	24.49	23.846	15.045
0.25	26.741	29.691	17.039	33.251	24.49	23.846	15.045
0.26	26.742	29.691	17.039	33.251	24.49	23.846	15.045
0.27	26.742	29.691	17.039	33.251	24.49	23.846	15.045
0.28	26.742	29.691	17.039	33.251	24.49	23.846	15.045
0.29	26.742	29.691	17.039	33.251	24.49	23.846	15.045
0.3	26.742	29.691	17.039	33.251	24.49	23.846	15.045
0.31	26.742	29.691	17.039	33.251	24.49	23.846	15.045
0.32	26.742	29.691	17.038	33.251	24.49	23.846	15.045
0.33	26.742	29.691	17.038	33.251	24.49	23.846	15.045
0.34	26.742	29.691	17.038	33.252	24.49	23.846	15.045
0.35	26.742	29.691	17.038	33.252	24.49	23.846	15.045
0.36	26.742	29.691	17.038	33.252	24.49	23.845	15.045
0.37	26.742	29.691	17.038	33.252	24.49	23.845	15.045
0.38	26.742	29.691	17.038	33.252	24.49	23.845	15.045
0.39	26.742	29.691	17.038	33.252	24.489	23.845	15.045
0.4	26.742	29.691	17.038	33.252	24.489	23.845	15.045
0.41	26.742	29.691	17.038	33.252	24.489	23.845	15.045
0.42	26.742	29.691	17.038	33.252	24.489	23.845	15.045
0.43	26.742	29.69	17.038	33.252	24.489	23.845	15.045
0.44	26.742	29.69	17.038	33.253	24.489	23.845	15.045
0.45	26.742	29.69	17.038	33.253	24.489	23.845	15.045
0.46	26.741	29.69	17.038	33.253	24.489	23.845	15.045
0.47	26.741	29.69	17.037	33.253	24.489	23.845	15.045
0.48	26.741	29.69	17.037	33.253	24.489	23.845	15.045

The graphs of sample temperature and programmed temperature of adsorbent over time generated from TGA were showed as below.
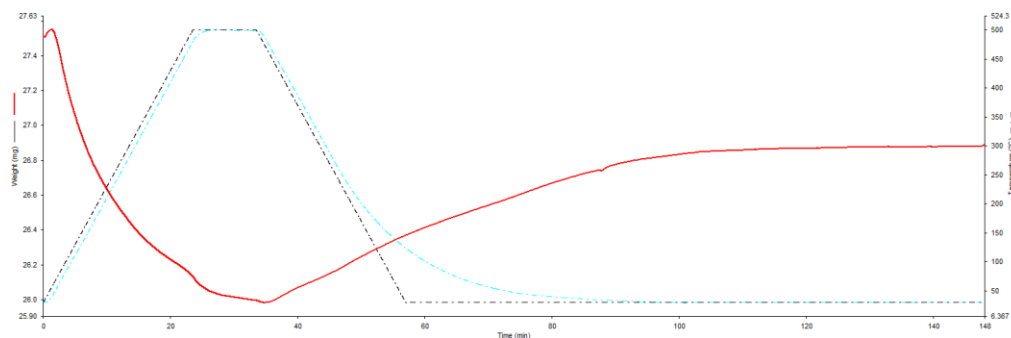

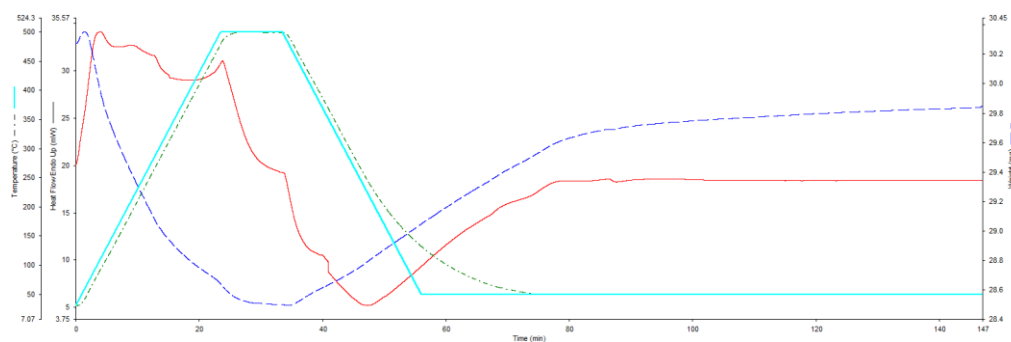Figure A-1: CO_2 Adsorption Process of R-MOR Zeolite at 30 °C.

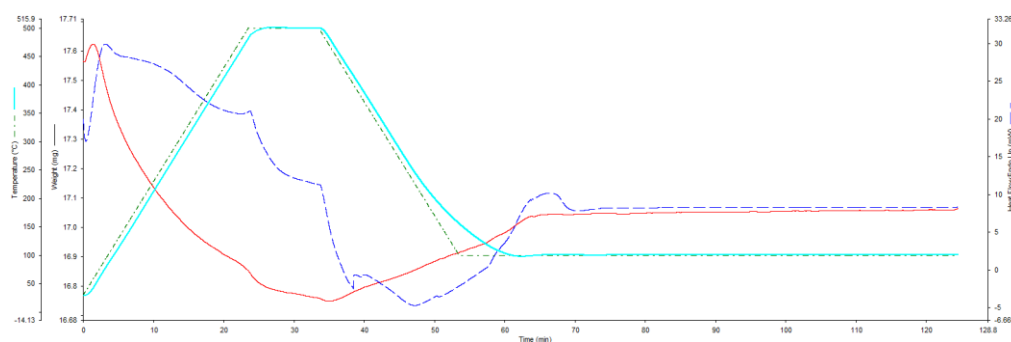Figure A-2: CO_2 Adsorption Process of R-MOR Zeolite at 50 °C.

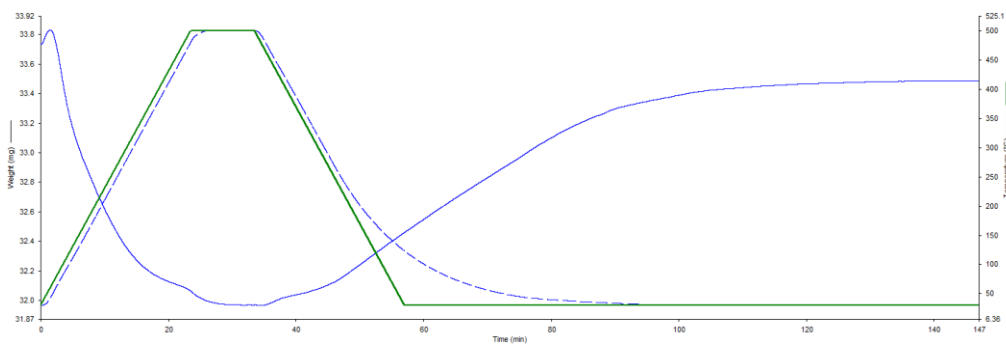Figure A-3: CO_2 Adsorption Process of R-MOR Zeolite at 100 °C.

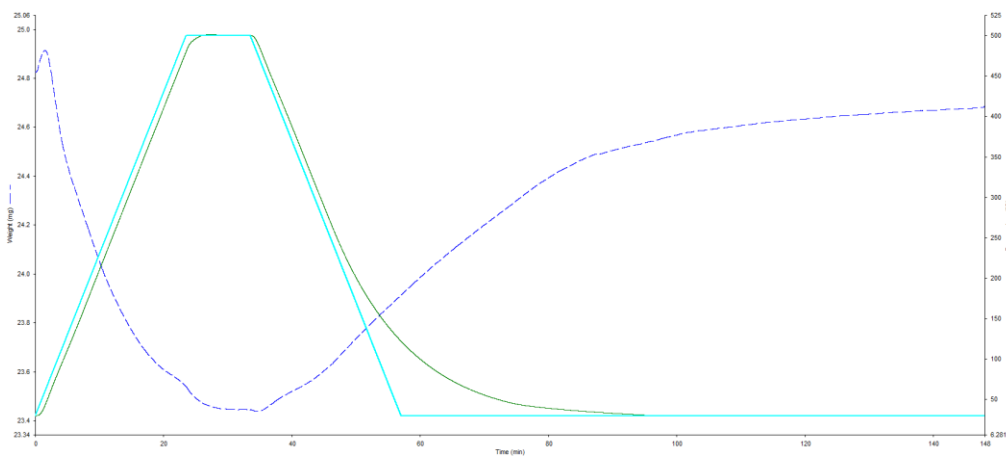Figure A-4: CO$_2$ Adsorption Process of K-MOR Zeolite at 30 °C.

Figure A-5: CO$_2$ Adsorption Process of Na-MOR Zeolite at 30 °C.
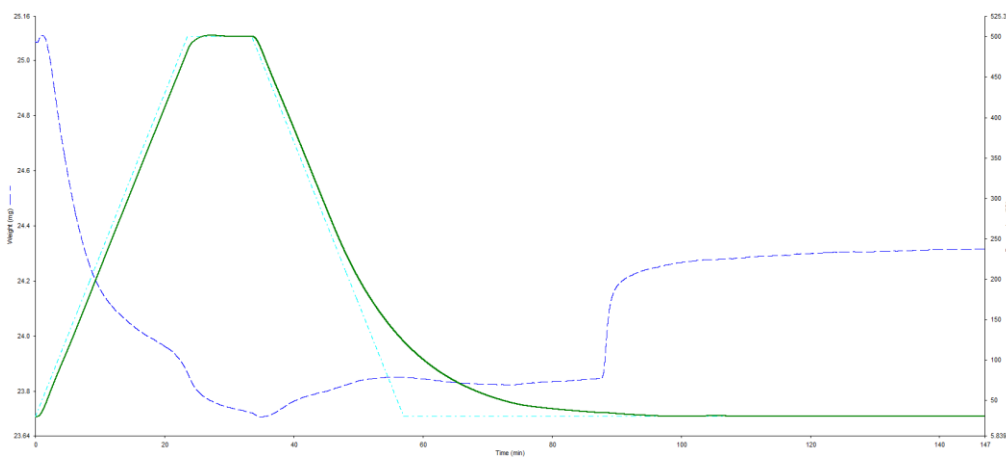

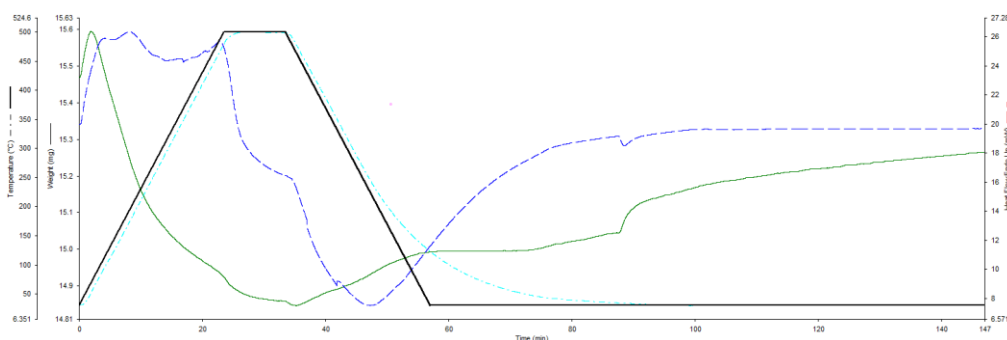Figure A-6: CO$_2$ Adsorption Process of Ca-MOR Zeolite at 30 °C.

Figure A-7: CO$_2$ Adsorption Process of Mg-MOR Zeolite at 30 °C.

Due to too large sets of raw data from TGA, part of the data for N$_2$ adsorption process of each adsorbent during cooling process of pre-treatment to desired temperature also showed in Table A-2. The data were extracted start from 36.51 minutes, since N$_2$ was estimated to be adsorbed by each adsorbent around that time.

Table A-2: TGA Raw Data for N$_2$ Adsorption of the Each Adsorbent during Cooling Process of Pre-Treatment to Desired Temperatures.

	Weight of Adsorbent (mg)					
	R-MOR			Na-MOR	Ca-MOR	Mg-MOR
Time (min)	30 °C	50 °C	100 °C	30 °C	30 °C	30 °C
36.51	26	28.535	16.758	23.462	23.715	14.854
36.52	26	28.535	16.758	23.462	23.716	14.854
36.53	26	28.535	16.758	23.462	23.716	14.854
36.54	26	28.536	16.758	23.463	23.716	14.854
36.55	26	28.536	16.758	23.463	23.716	14.854
36.56	26.001	28.536	16.758	23.463	23.716	14.854
36.57	26.001	28.536	16.759	23.463	23.716	14.854
36.58	26.001	28.537	16.759	23.463	23.716	14.854
36.59	26.001	28.537	16.759	23.463	23.716	14.854
36.6	26.001	28.537	16.759	23.464	23.716	14.855
36.61	26.001	28.537	16.759	23.464	23.716	14.855

Table A-2 (Continued)

36.62	26.002	28.538	16.759	23.464	23.716	14.855
36.63	26.002	28.538	16.759	23.464	23.717	14.855
36.64	26.002	28.538	16.759	23.464	23.717	14.855
36.65	26.002	28.538	16.759	23.464	23.717	14.855
36.66	26.003	28.539	16.76	23.465	23.717	14.855
36.67	26.003	28.539	16.76	23.465	23.717	14.855
36.68	26.003	28.539	16.76	23.465	23.717	14.855
36.69	26.003	28.539	16.76	23.465	23.717	14.855
36.7	26.003	28.54	16.76	23.465	23.717	14.855
36.71	26.004	28.54	16.76	23.466	23.717	14.856
36.72	26.004	28.54	16.76	23.466	23.718	14.856
36.73	26.004	28.54	16.76	23.466	23.718	14.856
36.74	26.004	28.54	16.761	23.466	23.718	14.856
36.75	26.004	28.541	16.761	23.466	23.718	14.856
36.76	26.004	28.541	16.761	23.466	23.718	14.856
36.77	26.005	28.541	16.761	23.467	23.718	14.856
36.78	26.005	28.541	16.761	23.467	23.718	14.856
36.79	26.005	28.542	16.761	23.467	23.718	14.856
36.8	26.005	28.542	16.761	23.467	23.718	14.856
36.81	26.006	28.542	16.761	23.467	23.719	14.856
36.82	26.006	28.542	16.761	23.467	23.719	14.856
36.83	26.006	28.543	16.762	23.468	23.719	14.856
36.84	26.006	28.543	16.762	23.468	23.719	14.857
36.85	26.006	28.543	16.762	23.468	23.719	14.857
36.86	26.006	28.543	16.762	23.468	23.719	14.857
36.87	26.007	28.544	16.762	23.468	23.719	14.857
36.88	26.007	28.544	16.762	23.469	23.719	14.857
36.89	26.007	28.544	16.762	23.469	23.719	14.857
36.9	26.007	28.544	16.762	23.469	23.72	14.857
36.91	26.007	28.545	16.762	23.469	23.72	14.857
36.92	26.008	28.545	16.762	23.469	23.72	14.857
36.93	26.008	28.545	16.763	23.47	23.72	14.857

APPENDIX B: Calculation of Adsorption Capacity, Adsorption Rate and
CO_2/N_2 Selectivity

The adsorption capacity and rate of adsorbate were calculated based on Eq. 5.1
and Eq. 5.2.

$$q_i = \frac{(M_t - M_0) \times 1000}{M_o \times MW_i} \tag{5.1}$$

$$q'_i = \frac{(M_t - M_0) \times 1000}{M_o \times MW_i \times t} \tag{5.2}$$

where

q_i = CO_2 adsorption capacity

q'_i = CO_2 adsorption rate

M_t = Mass of adsorbent at time t, mg

M_0 = Initial mass of adsorbent before CO_2 adsorption, mg

MW_i = Molecular weight of component i, mg·mmol^{-1}

t = Time, min

The data for CO_2 adsorption process for R-MOR zeolite at 30 ºC were showed.
Given,

$M_0 = 26.739$ mg

$M_t = M_{(0.48 \text{ min})} = 26.741$ mg

$t = 0.48$ min

The calculation of CO_2 adsorption capacity and CO_2 adsorption rate:

$$q_{CO_2} = \frac{(26.741 - 26.739) \times 1000}{26.739 \times 44.01}$$

$$= 0.001699548 \text{ mmol·g}^{-1}$$

$$q'_{CO_2} = \frac{(26.741 - 26.739) \times 1000}{26.739 \times 44.01 \times 60}$$

$$= 2.83258 \times 10^{-5} \text{ mmol·g}^{-1}\text{·min}^{-1}$$

The data for N_2 adsorption process for R-MOR zeolite during cooling process of pre-treatment to 30 ºC were showed.

Given,

$M_0 = M_{(36.51 \text{ min})} = 26$ mg

$M_t = M_{(36.93 \text{ min})} = 26.008$ mg

The calculation of N_2 adsorption capacity:

$$q_{N_2} = \frac{(26.008 - 26) \times 1000}{26 \times 28.0134}$$

$$= 0.010983754 \text{ mmol} \cdot \text{g}^{-1}$$

The CO_2/N_2 selectivity was calculated based on Eq. 5.3.

$$CO_2/N_2 \text{ selectivity} = \frac{q_{CO_2}/p_{CO_2}}{q_{N_2}/p_{N_2}} \qquad (5.3)$$

where

$q_{N_2} = N_2$ adsorption capacity

$p_{CO_2} = $ Partial pressure of CO_2

$p_{N_2} = $ Partial pressure of N_2

For R-MOR zeolite, the maximum CO_2 and N_2 adsorption capacity at 30 ºC were 0.119818143 mmol/g and 1.020116197 mmol/g respectively. It was assumed that the $p_{CO_2} = p_{N_2}$. The calculation CO_2/N_2 selectivity:

$$CO_2/N_2 \text{ selectivity} = \frac{0.119818143 \text{ mmol/g}}{1.020116197 \text{ mmol/g}}$$

$$= 0.117455387$$

APPENDIX C: Calculation for XRD

Data from R-MOR zeolite, peak number 12 was used for sample calculation.

Given,

2 Theta, 2θ =22.0693º

Full Width at Half Maximum, $FWHM$ = 1.0763º

λ = Wavelength of X−ray, 0.15406 nm (CuKα)

Convert 2 Theta from degree to radian,

$$2 \text{ Theta}, 2\theta = 22.0693 \times \frac{\pi}{180°}$$
$$= 0.385182 \text{ rad}$$
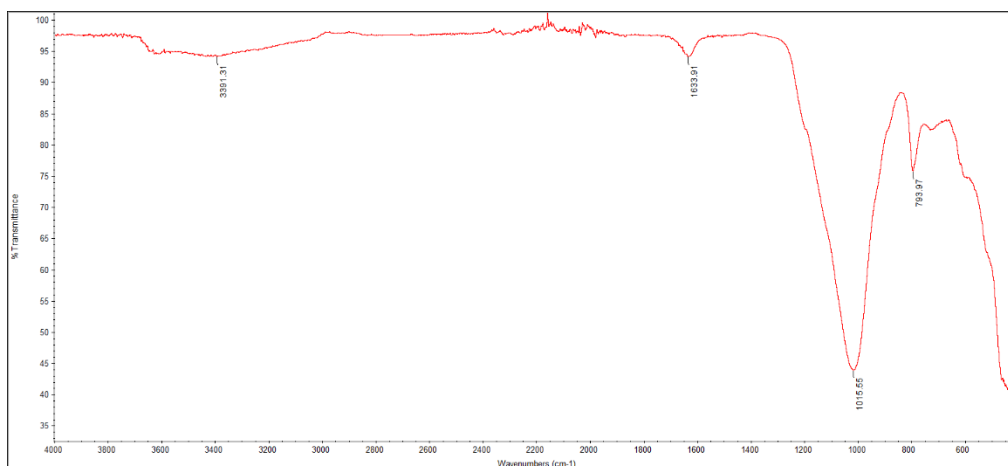
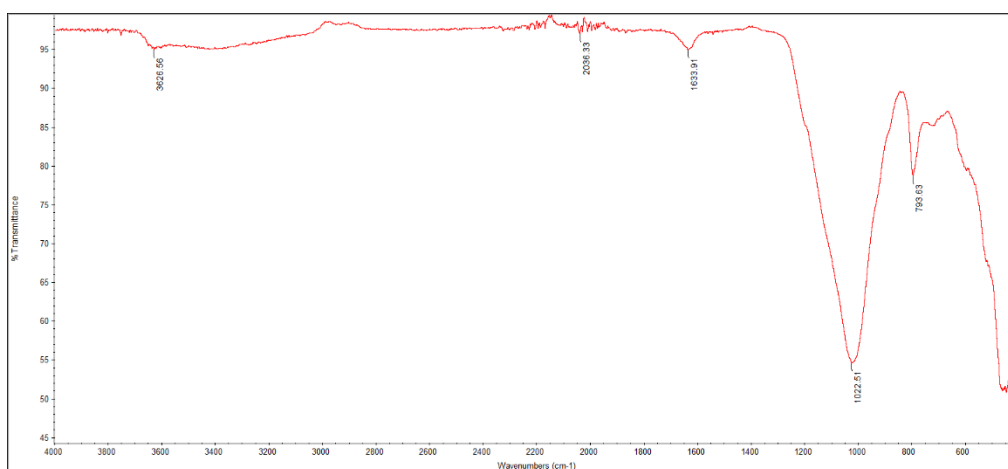Convert Full Width at Half Maximum from degree to radian,

$$\text{Full Width at Half Maximum}, \text{FWHM} = 1.0763 \times \frac{\pi}{180°}$$
$$= 0.018785 \text{ rad}$$

Calculate crystallite size by using Scherrer's equation,

$$Crystallite\ size, d_x = \frac{0.94\lambda}{FWHM \cdot cos\theta}$$
$$= \frac{0.94(0.15406 \text{ nm})}{0.018785 \cdot \cos(\frac{0.385182}{2})}$$
$$= 7.854374 \text{ nm}$$

APPENDIX D: FTIR results

Figure D-1: IR Septra of R-MOR zeolite after CO_2 Adsorbed at 30 °C.

Figure D-2: IR Septra of R-MOR zeolite after CO_2 Adsorbed at 50 °C.
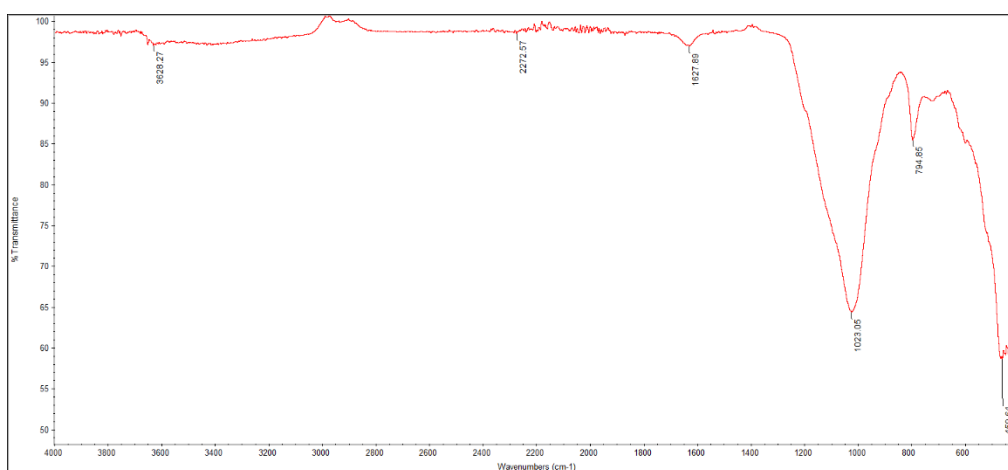
Figure D-3: IR Septra of R-MOR zeolite after CO_2 Adsorbed at 100 °C.

APPENDIX E: EDX Results

Table E-1: R-MOR zeolite.

Elements	Atomic Percentage (At %)					
	K	Na	Ca	Si	Al	O
Spot 1	1.25	0.5	0.34	31.65	6.12	60.15
Spot 2	1.83	1.14	0.91	29.29	6.3	60.54
Spot 3	1.7	0.87	0.65	30.66	6.93	59.2
Spot 4	1.24	0.61	0.4	31.67	5.32	60.76
Spot 5	1.68	0.75	1.04	31.1	6.87	58.56
Average Distribution	1.54	0.774	0.668	30.874	6.308	59.842

Table E-2: Na-MOR zeolite.

Elements	Atomic Percentage (At %)					
	K	Na	Ca	Si	Al	O
Spot 1	1.27	2.19	0.36	33.01	5.68	57.5
Spot 2	1.71	1.37	0.6	33.74	5.67	56.91
Spot 3	1.22	2.09	0.5	33.31	5.92	56.96
Spot 4	1.1	2.03	0.39	33.39	5.72	57.38
Spot 5	1.21	2.44	0.53	32.92	5.66	57.24
Average Distribution	1.302	2.024	0.476	33.274	5.73	57.198

Table E-3: K-MOR zeolite.

Elements	Atomic Percentage (At %)					
	K	Na	Ca	Si	Al	O
Spot 1	3.29	0.4	0.22	32.23	5.84	58.01
Spot 2	3.59	0.76	0.26	32.28	6.11	57
Spot 3	3.16	0.7	0.3	32.97	5.87	56.99
Spot 4	3.98	0.83	0.52	34.47	6.22	53.98
Spot 5	3.79	0.73	0.39	32	5.89	57.2
Average Distribution	3.562	0.684	0.338	32.79	5.986	56.636

Table E-4: Ca-MOR zeolite.

Elements	Atomic Percentage (At %)					
	K	Na	Ca	Si	Al	O
Spot 1	1.37	0.84	1.29	36.3	5.5	54.7
Spot 2	1.51	0.29	1.24	30.97	6.18	59.8
Spot 3	1.12	0.35	2.2	33.91	6.45	55.97
Spot 4	1.09	0.4	2.18	32.16	6.37	57.8
Spot 5	1.49	0.47	1.59	30.08	6.3	60.08
Average Distribution	1.316	0.47	1.7	32.684	6.16	57.67

Table E-5: Mg-MOR zeolite.

Elements	Atomic Percentage (At %)						
	K	Na	Ca	Mg	Si	Al	O
Spot 1	1.57	0.71	0.42	1.07	35.16	6.91	54,17
Spot 2	1.19	1.23	0.47	0.79	33.19	6.21	56.92
Spot 3	1.24	1.48	0.46	0.65	32.8	6.4	56.96
Spot 4	1.14	0.71	0.3	1.16	30.15	7.05	59.5
Spot 5	1.7	0.98	0.38	1.08	32.26	6.75	56.85
Average Distribution	1.368	1.022	0.406	0.95	32.712	6.664	57.5575